

1 **Pacific Southern Ocean coccolithophore-derived particulate**
2 **inorganic carbon (PIC): A novel comparative analysis of in-situ and**
3 **satellite-derived measurements**

4 Mariem Saavedra-Pellitero¹, Karl-Heinz Baumann², Nuria Bachiller-Jareno¹, Harold Lovell¹, Nele
5 Manon Vollmar^{2,3}, Elisa Malinverno⁴

6
7 ¹School of the Environment, Geography and Geosciences, University of Portsmouth, Portsmouth, PO1 3QL, United Kingdom

8 ²Department of Geosciences, University of Bremen, 28334, Bremen, Germany

9 ³NORCE Norwegian Research Centre AS, NORCE Climate & Environment, 5007, Bergen, Norway and Bjerknes Centre for
10 Climate Research, Bergen, Norway

11 ⁴Department of Geological Sciences and Geotechnologies, Milano-Bicocca University, 20126, Milan, Italy

12
13 *Correspondence to:* Mariem Saavedra-Pellitero (mariem.saavedra-pellitero@port.ac.uk)

14 **Abstract.**

15 Polar plankton communities are already experiencing the impact of ocean acidification and global warming. Coccolithophores
16 are the main type of calcifying phytoplankton in the Southern Ocean (SO) and they play a key role in the carbon cycle through
17 the production of particulate organic, and inorganic carbon (PIC). Coccolithophores account for most of the optical PIC
18 backscattering in the sea, so remote sensing is potentially an excellent monitoring tool. However, in situ measurements in the
19 SO are sparse in space and time due to the harsh weather conditions.

20 Here, we combine micropalaeontology and remote-sensing to evaluate critical discrepancies between coccolithophore and
21 satellite-derived PIC in the Pacific SO in non-bloom conditions. Plankton samples were collected from two latitudinal
22 transects: from New Zealand to Antarctica (December 2004-January 2005) and across the Drake Passage (February-March
23 2016). Coccolithophore species specific PIC estimates were compared, based on 1) Scanning Electron Microscope cocolith
24 morphometric analyses and 2) remote sensing PIC values acquired from NASA's Ocean Color Web service. Considering that
25 the SO is the cloudiest region on Earth (which limits the amount of satellite data available), in-situ and satellite-
26 derived PIC datasets show very good agreement in both transects, particularly in the Subantarctic and Polar Front zones.
27 *Emiliana huxleyi* morphogroup B substantially contributes to the sea-surface PIC content south of the Subantarctic Front in
28 both transects, whereas *E. huxleyi* types A, A overcalcified, and other taxa (e.g. *Calcidiscus leptoporus*), only contribute to
29 coccolithophore PIC in the northernmost stations.



30 Of particular interest are strong peaks in satellite-derived PIC south of the Polar Front, which do not show up in the
31 coccolithophore data. We suggest that the high reflectance signal from this southernmost region (which could have been
32 initially attributed to coccolithophores) may be due to the prevalence of small opal particles or unknown highly reflective
33 particles (such as *Phaeocystis* aggregations or suspended sediment). Our observations highlight the importance of satellite
34 products for estimating global PIC levels, while emphasizing the critical need for validation through field samples. This work
35 contributes to our understanding of coccolithophore PIC dynamics in the “data desert” Pacific SO, offering valuable insights
36 for both remote sensing applications and the broader field of marine science.

37 **1 Introduction**

38 Coccolithophores are a major component of calcifying phytoplankton communities in the Southern Ocean (SO) (e.g. Saavedra-
39 Pellitero et al., 2014; Saavedra-Pellitero et al., 2019; Malinverno et al., 2015; Charalampopoulou et al., 2016; Rigual Hernández
40 et al., 2020a) and play an important and complex role in the carbon cycle through the production of particulate inorganic
41 carbon (PIC) and particulate organic carbon (POC) (e.g. Rost and Riebesell, 2004; Salter et al., 2014). These haptophyte algae
42 produce an external covering (coccosphere) of interlocking calcite platelets (coccoliths). This process decreases the alkalinity
43 of surface waters, thereby reducing the uptake of CO₂ from the atmosphere into the surface ocean, thus acting in opposition to
44 carbon sequestration by the biological carbon pump (Rost and Riebesell, 2004). Previous work has suggested that calcification
45 during blooms of the coccolithophore *Emiliania huxleyi*, aka *Gephyrocapsa huxleyi* (Bendif et al., 2023), might alter the air-
46 sea flux of CO₂ (e.g. Harlay et al., 2010; Shutler et al., 2013), although to date, the impact of this has mostly only been explored
47 on a limited regional basis (e.g. Balch et al., 2016).

48
49 Since the early days of satellite-based colour measurements of the oceans, large coccolithophore blooms have been visible as
50 highly reflective regions in satellite images (e.g. Holligan et al., 1983). Coccolithophores, and their detached coccoliths, are
51 strongly optically active and notably affect the optical budget of the surface ocean, and can thus be seen from space using
52 satellite remote sensing (Smyth et al., 2002; Tyrrell and Taylor, 1996). Coccolithophores are responsible for most of the optical
53 PIC backscatter in the ocean; the other, larger PIC particles associated with foraminifera and pteropods provide negligible
54 backscatter per unit mass and therefore have minimal optical impact (Balch et al., 1996). In general, detached coccoliths
55 account for 10-20 % of the light backscattered from the sea under non-bloom conditions, whereas under bloom conditions it
56 can be more than 90 % (Balch et al., 1991; Balch et al., 1999). The strong scattering properties of the coccolithophores and the
57 associated PIC lead to enhanced reflection in the entire visible spectrum (400-700 nm). Gordon et al. (2001) and Balch et al.
58 (2005) developed algorithms to estimate the PIC concentration in the surface layer of the water column from the radiance
59 emanating from the water. The relationship between inherent optical properties and the resultant light fields is well understood
60 (e.g. Mitchell et al., 2017). The difficulty lies in understanding the combined effects of different in-water constituents on the
61 inherent optical properties, and ultimately, the underwater light fields. While there have been many advances in this area (e.g.



62 Babin et al., 2003a; Babin et al., 2003b; Devred et al., 2006), there will always be some error in calculating these relationships.
63 For example, some authors have shown that satellite ocean-colour-based PIC estimates did not match in situ (ship-based)
64 observations and that satellite-derived PIC can be overestimated in Antarctic waters (e.g. Holligan et al., 2010; Trull et al.,
65 2018). One potential source of error is that aquamarine waters characterized by high reflectance of light can also be caused by
66 suspended sediment and even opal particles, such as fragments of diatom frustules (e.g. Broerse et al., 2003).

67
68 Satellite data has played a key role in showing the importance of the increasing *E. huxleyi* blooms in the world's oceans (e.g.
69 Balch et al., 1991; Iida et al., 2002; Siegel et al., 2007; Neukermans et al., 2018; for further citations see review in Balch and
70 Mitchell, 2023). This is relevant for monitoring changes at a global scale and to detect seasonal patterns as well as interannual
71 variations (e.g. Smyth et al., 2004; Winter et al., 2014; Rigual-Hernández et al., 2020a) or trends, with the ultimate goal of
72 feeding information into models for climate projections in the context of global warming and ocean acidification (e.g.
73 Neukermans et al., 2018; Krumhardt et al., 2019). Recent concerns about climate change and ocean acidification pointed to *E.*
74 *huxleyi* as a target cosmopolitan species to understand the biological response. Expansion or reduction of the biogeographic
75 range, changes in coccolith calcification and preservation are possible responses that were observed in water and sediment
76 samples. The high-latitude distribution of *E. huxleyi* has undergone a recent poleward expansion in both the northern (Rivero-
77 Calle et al., 2015) and southern hemisphere (Cubillos et al., 2007; Winter et al., 2014). However, data from the SO is rather
78 limited and there are not enough in situ measurements to unravel the complex dynamic relationships between *E. huxleyi*
79 distribution and the frontal dynamics of the Antarctic Circumpolar Current (ACC). Significant zonal differences are shown in
80 the relationship between coccolithophore data and ACC frontal positions across the different sectors of the SO, but no strong
81 evidence of recent expansion on a circumpolar scale has been identified (Malinverno et al., 2015).

82
83 The band of high reflectance and elevated PIC waters observed in the SO between 30° - 60° S during Austral summer, known
84 as “the Great Calcite Belt”, has been linked to a region of increased seasonal concentration of coccolithophores (Balch et al.,
85 2011; Balch et al., 2016). Comparisons of in situ and remote sensing measurements of PIC have been undertaken in the Atlantic
86 and Indian sectors of the SO for coccolithophore bloom conditions (e.g. Balch et al., 2014; Balch et al., 2016; Poulton et al.,
87 2011). Nonetheless, this type of comparison is very limited in specific areas of the globe (such as the vast Pacific sector of the
88 SO) but also in non-bloom coccolithophore conditions. This is partially due to the fact that available coccolithophore
89 concentrations are sparse in space and time in the SO. Most of the subpolar studies focus on coccospheres, whilst there are
90 scarce data on free coccoliths (Mohan et al., 2008).

91
92 Changes in the calcification of *E. huxleyi* coccoliths have been shown in sub-Antarctic waters, (Cubillos et al., 2007), with
93 different morphotypes representing the genotypic response to different water chemistry. Beaufort et al. (2011) and Horigome
94 et al. (2014) point to an environmental control on different calcification of *E. huxleyi*. Several estimates of coccolith-PIC exist:
95 estimation of coccolith-mass from coccolith volume calculated from coccolith-size (Young and Ziveri, 2000; Beuvier et al.,



96 2019) or estimation of coccolith-calcite mass through calibration of its birefringence signal at the light microscope (Beaufort,
97 2005; Bollmann, 2014; Fuertes et al., 2014). Direct comparisons between coccolith-PIC and sea surface water scattering in the
98 SO have targeted areas of coccolithophore bloom (Holligan et al., 2010; Poulton et al., 2011; Balch et al., 2014; Oliver et al.,
99 in press) but so far this has not been undertaken for non-bloom areas.

100

101 Here, we calculate the contribution of *E. huxleyi* and minor coccolithophore species to sea surface PIC along two latitudinal
102 transects across the ACC fronts, a New Zealand transect and a Drake Passage transect, where coccosphere concentrations are
103 below 1.3×10^5 and 1.5×10^5 cells/L, respectively corresponding to non-bloom to outer bloom conditions (Poulton et al., 2011).
104 Our aims are: 1) to define the contribution of the different coccolithophore species to PIC in surface waters, 2) to assess the
105 degree of calcification of the different *E. huxleyi* morphotypes along the transect and 3) to assess the source of high reflectance
106 in the Antarctic Zone, south of the Southern ACC Front, along our investigated transect.

107 **2 Oceanographic setting, phytoplanktonic communities, and study area**

108 The SO is a high-nutrient, low-chlorophyll area in the Southern Hemisphere (e.g. De Baar et al., 1995) that connects all the
109 main oceans through the strong and eastward flowing ACC. In the SO, there are a number of oceanographic fronts characterized
110 by increased horizontal transport and rapid changes in water properties (Orsi et al., 1995; Klinck and Nowlin, 2001). The ACC
111 is bounded by the Subtropical Front (STF) in the north, which separates it from the warmer and saltier waters of the subtropics,
112 and its southern edge is marked by the Southern Boundary, which separates it from subpolar cold, silicate-rich waters (Orsi et
113 al., 1995). Although the ACC flow is mostly driven by the westerly winds, the position of the fronts varies spatially and
114 seasonally and it is also controlled by steep topographic features, such as oceanic plateaus or ridges (Gordon et al., 1978).
115 South of the STF, the Subantarctic Front (SAF) separates the Subantarctic Zone (SAZ) and the Polar Frontal Zone (PFZ) (Fig.
116 1). The location of the SAF is indicated by a strong thermal gradient and by the rapid descent of a salinity minimum associated
117 with the Antarctic Intermediate Water, from the surface in the PFZ ($S < 34$ ‰) to depths greater than 300 m in the SAZ ($S < 34.20$
118 ‰) (Orsi et al., 1995; Whitworth, 1980). South of the SAF, the prominent Polar Front (PF) separates the PFZ and the Antarctic
119 Zone (AZ). The PF represents the northernmost extent of the 2°C isotherm at 200 m depth and corresponds to a 2°C gradient
120 in sea surface temperature (Orsi et al., 1995). The Southern ACC Front is characterized by temperatures below 0°C at the
121 minimum temperature in the sub-surface (< 150 m) and above 1.8°C at the maximum temperature at depths > 500 m (Orsi et
122 al., 1995). A more detailed description of the property indicators at each SO front can be found in Orsi et al. (1995).

123

124 Coccolithophores dominate the SO phytoplankton communities, especially in the SAZ, where they reach relatively high
125 numbers and diversity (e.g. Gravalosa et al., 2008; Saavedra-Pellitero et al., 2014; Malinverno et al., 2015; Charalampopoulou
126 et al., 2016; Saavedra-Pellitero et al., 2019; Rigual Hernández et al., 2020a). On the other hand, diatoms and other siliceous
127 microfossils dominate south of the PF (e.g. Saavedra-Pellitero et al., 2014; Malinverno et al., 2016; Cárdenas et al., 2018). The



128 coccolithophore abundance and diversity in the Drake Passage drastically drop from north to south, with the oceanographic
129 fronts appearing to act as ecological boundaries (Saavedra-Pellitero et al., 2019), whereas the total coccolithophore abundance
130 is highest in the PFZ south of New Zealand (Malinverno et al., 2015). Similar marked shifts at the SAF and PF in
131 coccolithophore number, community composition, and diversity occurring were also previously noted in other sectors of the
132 SO (e.g. Mohan et al., 2008; Gravalosa et al., 2008; Saavedra-Pellitero et al., 2014; Balch et al., 2016; Charalampopoulou et
133 al., 2016) and are in accordance with previous observations in both transects (Malinverno et al., 2015; Saavedra-Pellitero et
134 al., 2019). In particular, the PF (Drake Passage) and the Southern ACC Front (New Zealand transect) constitute natural sharp
135 barriers marked by a clear drop in the number of *E. huxleyi*, which often is the only species found in the PFZ and almost always
136 or only occurs here as B morphogroup (type B/C and O). Furthermore, a general southwards decreasing trend in *E. huxleyi*
137 mass, linked to a latitudinal trend from more calcified *E. huxleyi* (A morphogroup) to weakly calcified morphotypes (B
138 morphogroup), was already recorded across the Drake Passage (Saavedra-Pellitero et al., 2019).

139

140 **3 Materials and methods**

141 **3.1 Sampling considerations and morphometrics**

142 **3.1.1 The New Zealand transect**

143 Fifty-eight surface water samples were collected from the ship's pump of the R/V *Italica* (at ca. 3 m water depth) from 46.81°S
144 to 69.98°S during the XX Italian Expedition from New Zealand to Antarctica (31st December 2004- 6th January 2005). Details
145 on sample locations, sampling volume, coccolithophore and coccolith counts can be found in Malinverno et al. (2015).

146

147 From these samples we selected a total of 13 samples for Scanning Electron Microscope (SEM, Vega Tescan at the University
148 of Milano-Bicocca) morphometric analyses of *E. huxleyi* as being representative of the different *E. huxleyi* populations from
149 the various biogeographic zones across the ACC (Fig. 1). For each sample, 30-50 images of *E. huxleyi* free coccoliths and
150 coccospheres were collected as encountered during filter scanning (377 images in total, Table 1S in Supplementary Material).
151 Distal shield length and width, tube thickness, and number and thickness of distal shield elements were manually measured
152 using the ImageJ software (Schneider et al., 2012) in micrometers (μm) using the scalebar of the SEM images (Fig. 2).

153 **3.1.2 The Drake Passage transect**

154 Nineteen water samples were collected on a transect at the western end of the Drake Passage (55.44°S to 61.75°S) during
155 Polarstern Expedition PS97 from 24th February 2016 to 5th March 2016 (Fig. 1). These selected plankton samples were
156 obtained using a rosette sampler with 24×12 L Niskin bottles (Ocean Test Equipment Inc.) attached to a CTD Seabird



157 SBE911plus device (Lamy, 2016). The bottles were fired by a SBE32 carousel and just the shallowest samples, from 5, 10 and
158 20 m water depth, were considered in this work.

159
160 A total of 203 images of *E. huxleyi* coccospheres were taken from the samples in the Drake Passage while scanning the filters
161 within the SEM (Table 2S in Supplementary Material). Coccoliths were measured using the Coccobiom2 macro (Young, 2015)
162 in the software programme Fiji, an image processing package based on ImageJ (Schindelin et al., 2012). Measurements were
163 made in micrometers (μm), based on the scale bar of the SEM images. Note that they were scaled to 100% with a Coccobiom2
164 SEM calibration of 1.09 and the specific magnification.

165 3.2 Coccolithophore PIC estimates

166 Species-specific coccolith-PIC (in pMol) was estimated following the volume calculation of Young and Ziveri (2000)

167
168
$$PIC = (2.7 \times Ks \times L^3) \div 100 \quad \text{[equation 1]}$$

169
170 where:

171 2.7 = density of calcite;

172 Ks = species-specific shape factors, as provided by Young and Ziveri (2000) and modified for *E. huxleyi* according to the
173 degree of calcification obtained for each morphotype (see Table 1);

174 L = coccolith mean length from measurements in the case of *E. huxleyi*. For minor species, we considered the averaged
175 coccolith length provided by Young and Ziveri (2000).

176 100 = molecular weight of calcite

177
178 Measurements of the distal shield diameters of *Calcidiscus leptoporus* the second most abundant species, that is significantly
179 larger than *E. huxleyi*, were made on different samples offshore New Zealand, corresponding to the highest abundances of this
180 taxa (Table 1 and Table 3S in Supplementary Material). The coccolith-PIC contribution for each sample was calculated by
181 applying the obtained species-specific calcite quota to the abundances of species and morphotype (i.e., coccospheres/L) from
182 Malinverno et al. (2015) and Saavedra-Pellitero et al. (2019). In the New Zealand transect, the single / double coccolith layers
183 were considered in the estimates (Table 1S in Supplementary Material), while in the Drake Passage transect, where this
184 information was not available, an average was considered based on own observations (Table 1 and Table 4S in Supplementary
185 Material).

186 We also calculated the relative tube width' in *E. huxleyi* as a size-independent index to estimate the degree of calcification in
187 this taxa following a modification of the index proposed by Young et al. (2014) (Fig. 2):

188
189
$$\text{Relative tube width}' = (2 \times \text{tube width}) \div \text{coccolith length} \quad \text{[equation 2]}$$



190

191 **3.3 Satellite-derived PIC data**

192 Daily, 8-daily and monthly L-3 MODIS-derived PIC values (mol m^{-3}) (NASA Ocean Biology Processing Group, 2022, 2023a)
193 with a spatial resolution of 4 km, covering both the sampling period and the geographical extent of each transect, were acquired
194 from NASA's Ocean Color Web service as individual netCDF files for each timestamp. The date ranges of each PIC period
195 are summarised in Table 2.

196

197 Daily, 8-daily (going forward, referred to as weekly) and monthly values of PIC were extracted for all sampling locations in
198 both transects (Figures 1S and 2S in Supplementary Material). Processing of the PIC data was done with a Python script that
199 used NetCDF4 and other libraries commonly used for data analysis such as Pandas. The PIC data processing was done in
200 JASMIN Notebook Service (<https://jasmin.ac.uk/>).

201

202 One limitation of optical remote sensing products is that they cannot provide a reliable signal under cloudy conditions.
203 Combined with other conditions that interfere with the detection of water-leaving radiances (NASA Ocean Biology Processing
204 Group, 2023a), daily PIC grids have a high number of missed observations, or gaps, which prevent us from getting daily
205 satellite-derived PIC values of the sampling dates for most sample locations in both transects. Based on this fact, weekly and
206 monthly satellite-derived PIC values were therefore used in the analysis.

207 **3.4 Statistical analysis**

208 A principal component analysis (PCA) was performed on the *E. huxleyi* morphometric dataset (including samples from both
209 transects) using PAST™ software version 4.13 (Hammer et al., 2001). The morphometric data considered here were: coccolith
210 length, coccolith width (minor), distal shield element (or T-element) width, number of T-elements and tube width
211 measurements. The main aim of the PCA is to find hypothetical components that account for the maximum variance in the
212 multivariate dataset (Davis, 1986; Legendre and Legendre, 1998; Harper, 1999). These components are linear combinations
213 of the original variables (Hammer et al., 2001). The first Principal Component explains the highest variance, followed by the
214 subsequent components which explain the next largest variances. All the measurements were log-transformed prior to the PCA
215 to avoid skewness.

216 **4 Results**

217 **4.1 Coccolith-PIC versus satellite-derived PIC**

218 *Emiliania huxleyi* is clearly the dominant species in the coccolithophore assemblage of the Pacific SO (Malinverno et al., 2015;
219 Saavedra-Pellitero et al., 2019) with abundances of 1.4×10^5 coccospheres/L right south of the SAF in the New Zealand transect



220 and $1.5 \cdot 10^5$ coccospheres/L in the Chilean SAZ (PS97/034-2) and it is also the main contributor to sea-surface PIC (Figs. 3
221 and 4). *Calcidiscus leptoporus* (mostly *Calcidiscus leptoporus* ssp. *leptoporus*) is the second most abundant species and makes
222 significant contributions to the coccolithophore PIC at certain locations (up to $1.4 \cdot 10^4$ cells/L in the New Zealand transect
223 and $1.4 \cdot 10^3$ cells/L in the Drake Passage, Figs. 3 and 4) (Malinverno et al., 2015; Saavedra-Pellitero et al., 2019). *Calcidiscus*
224 *leptoporus* generally represents on average 13.4% of the total coccolithophore PIC in the New Zealand transect and 3.8% in
225 the Drake Passage, but can occasionally reach maximum PIC contributions of 57.5% (at the TR007 station, in the SAZ) and
226 of 23.3% (at the PS97/038-1 in the PFZ) (Fig. 5).

227
228 A minor contribution from less abundant or rare species occurs just in the northern SAZ of both transects, where diversity is
229 higher (for species list see Malinverno et al., 2015; Saavedra-Pellitero et al., 2019), with a poleward decreasing trend and
230 almost no contribution south of the SAF (Fig. 5). *Emiliana huxleyi* is solely responsible for almost all of the coccolith-PIC in
231 the PFZ, but its contribution decreases at the PF (in the Drake Passage) or Southern ACC Front (in the New Zealand transect,
232 ca. 63.7°S) and south of it.

233 Weekly and monthly MODIS-derived PIC at the sampling locations consistently overestimate PIC values by a factor of 2 to 5
234 with respect to in-situ values calculated from coccolith mass in the New Zealand transect (Fig. 3) and by occasionally an order
235 of magnitude in the Drake Passage (Fig. 4). Apart from the discrepancy in absolute values (and considering that there are
236 already inherent variations in the weekly compared to the monthly PIC estimates), there is a relatively good agreement in the
237 latitudinal satellite and coccolith-PIC trends in the SAZ and PFZ.

238 However at the PF (ca. 60°S in the Drake Passage) or to the south of it (ca. 62.5°S in the New Zealand transect), the satellite-
239 and the coccolith-PIC estimates became decoupled, with high reflectance but no coccolithophores in the AZ.

241 **4.2 Morphometries and mass estimates of *Emiliana huxleyi***

242 *Emiliana huxleyi* consist of different morphotypes that show a different and partly overlapping distribution along both
243 latitudinal transects (Malinverno et al., 2015; Saavedra-Pellitero et al., 2019). Type A is mostly restricted to the northern SAZ,
244 but it is occasionally present in the PFZ in the Drake Passage (Figs. 3, 4) and it is the only type within morphogroup A in this
245 study. Morphotypes belonging to the *E. huxleyi* morphogroup B (which includes morphotypes B, B/C, C and O) are present in
246 the SAZ and the PFZ, but they disappear south of the PF.

247
248 Morphometric measurements on coccoliths of *E. huxleyi* from the selected samples show that the length of types A, B/C-C
249 and O overlap in both transects (Fig. 6). In the Drake Passage, coccolith lengths range from 2.86 to 3.96 μm , with a mean
250 average of 3.49 μm for A type (including normal and overcalcified specimens), 2.87 to 4.11 μm for B type, 2.2 to 3.98 μm for
251 B/C-C types, 2.42 to 4.16 μm for O type, and an average of 2.98 μm for morphogroup B. In the New Zealand transect,



252 maximum axes range from 2.25 to 3.59 μm , with an average of 2.95 μm for *E. huxleyi* A type, 1.95 to 3.62 μm for B/C-C
253 types, 2.07 to 4.14 μm for O type, and an average of 2.87 μm for morphogroup B.

254

255 Figure 5 provides a latitudinal overview of morphometric data compared to the (averaged) degree of calcification. In the New
256 Zealand transect there are no significant changes in coccolith lengths except for a wide scatter of values characterizing the size
257 class distribution of each sample. This feature reflects the large variability in coccoliths size as observed on coccoliths from a
258 single coccosphere (Fig. 2e). However, in the Drake Passage transect, *E. huxleyi* coccoliths are notably larger offshore of Chile
259 (Fig. 6a).

260

261 *Emiliania huxleyi* masses calculated in the New Zealand transect range from 0.61 to 2.93 pg with an average of 1.47 pg per
262 coccolith belonging to the morphogroup A, and from 0.36 to 2.86 pg, with an average of 1.15 pg per placolith from
263 morphogroup B (Fig. 3c). In the Drake Passage the masses per coccolith for morphogroup A are almost double than in the
264 New Zealand transect, varying between 1.4 pg and 6.3 pg, with an average of 3 pg. The placolith masses in morphogroup B
265 range from 0.6 to 3.7 pg with a mean of 1.4 pg across the Drake Passage (Fig. 4c). Note that this data is shown in Figures 3
266 and 4, but the coccolith-PIC was calculated in this work using equation 1 and the average lengths mentioned in Table 1. The
267 coccolith-PIC estimated for *E. huxleyi* are generally lower in the New Zealand transect (average morphogroup A: 0.021 pmol
268 and B: 0.013 pmol) than in the in the Drake Passage (average morphogroup A: 0.034 pmol and B: 0.014 pmol).

269

270 We observed that some coccoliths are clearly overcalcified (see Figure 5 for an example), with a thick inner tube (up to 0.7
271 μm in sample PS97/018-1) that extends into the central area. Specimens belonging to the morphogroup A show a higher degree
272 of calcification than those belonging to morphogroup B, resulting not only in a thicker inner tube but also in thicker distal
273 shield T elements. The overcalcified coccospheres co-occur with normally-calcified ones but they are restricted to the
274 northernmost samples (Fig. 6). The relative tube width' (an index for calcification; Young et al., 2014), calculated using
275 equation 2, varies from 0.08 to 0.22 in morphogroup A and from 0.06 to 0.18 in B for the New Zealand transect. Values are
276 higher in the Drake Passage, ranging from 0.04 to 0.41 for *E. huxleyi* morphogroup A, and from 0.02 to 0.19 for morphogroup
277 B.

278

279 The variation in the degree of calcification (calculated using equation 2) is higher within each sample than along the New
280 Zealand transect (Fig. 3b), although overcalcified specimens (relative tube width' >0.22), typically represented by type A,
281 occur in the northernmost samples (Fig. 6b). Averaged relative tube width' shows increased values not only in the SAZ offshore
282 New Zealand, but also around 54 °S and in the PFZ (Fig 6b), which points to a certain degree of variation in the calcification
283 within morphotypes BC/C and O. A more marked N-S decrease in the relative tube width' values is observed in the Drake
284 Passage with notably higher values offshore of Chile (Figs. 3b and 6a), where relatively large and heavily calcified type A
285 coccospheres are present.



286

287 To better characterize *E. huxleyi* morphotypes in the study area we performed a PCA of the log-transformed morphometric
288 data. The first component, related to the tube width, explains 79.9% of the variance, and the second, related to length as well
289 as width (and to a lesser extent distal shield element width and number of T-elements), accounts for 11.5% (Fig. 7).

290 5. Discussion

291 5.1 PIC variability in the SAZ and PFZ

292 In the studied transects, the calculated coccolith-PIC and the satellite-derived PIC trends show quite good agreement in the
293 SAZ and PFZ, but there is a strong discrepancy in the AZ. Here we discuss potential factors influencing water-leaving radiance
294 in each of these areas.

295

296 The fact that satellite-derived data show consistently higher numbers than coccolith-PICs (Figs. 3 and 4) could be either due
297 to an overestimation of the satellite PIC values or to an underestimation of the species specific coccolith-PIC (i.e., coccolith-
298 calcite quotas). Additionally, the fact that the difference between satellite PICs and in situ values in the Drake Passage transect
299 is larger than in the New Zealand transect can be in part attributed to the fact that detached coccoliths (on top of coccospheres)
300 were only considered in the estimates for the New Zealand transect. Part of the disparity can be attributed to the different
301 spatial scale, considering the image pixel area vs. the discrete sampling. However, the fact that the overall trends are the same
302 in this region and that in situ measurements agree with the remote sensing data, could suggest that there is a satellite bias linked
303 to the algorithm (which could be easily adjusted for the region north of the SO). We are aware that the MODIS/Aqua Ocean
304 Color was re-processed in 2022 (NASA Ocean Biology Processing Group, 2023a) to incorporate updates in instrument
305 calibration, new ancillary sources and algorithm improvements but the validation of the PIC measurements is based just on a
306 very low number of in-situ measurements compared to other products (e.g., 1347 in situ measurements for Chlorophyll a and
307 just 42 for PIC, all of them in the Atlantic Ocean; NASA Ocean Biology Processing Group, 2023c, 2023b) .

308

309 The SAZ and PFZ are generally characterized by moderate coccolithophore concentration with limited contribution from other
310 biogenic particles (Figs. 3 and 4) (Malinverno et al., 2016; Saavedra-Pellitero et al., 2019). Given that *E. huxleyi* is the dominant
311 species in both transects and the most important contributor to pelagic PIC, we focused on its abundance, morphotype
312 distribution and calcite weight. Coccolith-PIC calculated in this study for *E. huxleyi* are generally in agreement with the calcite
313 content per coccolith obtained by Poulton et al. (2011) along the Patagonian Shelf and by Rigual Hernández et al. (2020a) in
314 the Australian & New Zealand sectors of the SO (see Tables 1 in those papers). Our PIC *E. huxleyi* estimates seem generally
315 higher than the estimates by Charalampopoulou et al. (2016) off southern Chile (0.015 pMol per coccolith) and across the rest
316 of Drake Passage (< 0.009 pMol).

317



318 On the other hand, our values are slightly lower than those obtained through the birefringence method SYRACO, an automated
319 system of coccolith recognition (SYstème de Reconnaissance Automatique de COccolithes) in the same latitudinal range (e.g.
320 Beaufort et al., 2011) and notably lower than Saavedra-Pellitero et al. (2019) across the Drake Passage using circularly
321 polarised light plus the C-Calcita software developed by Fuertes et al. (2014) (Fig. 8a). In order to explore this difference, we
322 calculated PICs in the Drake Passage using Saavedra-Pellitero et al. (2019) mass estimates for the same samples, considering
323 an average mass of 4.64 pmol for *E. huxleyi* ($n = 796$, standard deviation = 2.53) but without distinguishing different
324 morphotypes (Fig. 8b). The mass per coccolith of *E. huxleyi* using C-Calcita in the Drake Passage is 2.8 times higher than in
325 this work (mean of 1.66 pg in this work). We then used this factor to calculate the potential contribution of the rest of the
326 coccolithophore taxa (see Figure 8). Both N-S coccolith mass and PIC trends mirror each other, but the C-Calcita-derived PICs
327 tend to overestimate satellite values, except in a couple of locations. This can be attributed to the calibration of the coccolith
328 thickness within the software C-Calcita, which has been improved in recent years with the use of a calcite wedge instead of a
329 calcareous spine (e.g. Guitián et al., 2022). The differences in PIC could also be due to the fact that we are comparing in situ
330 values to monthly averages, and also smoothing data by considering averaged values when estimating coccolith-PICs
331 (especially length and number of coccoliths per coccosphere). In addition, sampling at slightly different times of the year may
332 also have an influence on the PIC values determined (Rigual Hernández et al., 2018; Rigual-Hernández et al., 2020a, b). An
333 increase in coccolith weight and size within morphotype B/C from December to August (but also from December to March)
334 was observed at a sediment trap station deployed at 61°S in the Australian sector of the SO south of Tasmania (Rigual
335 Hernández et al., 2018). Variations in light intensity in the mixed layer and increasing iron limitation were seen as the most
336 likely drivers of this change. This could explain differences in the carbonate masses of different transects.

337
338 Our measurements on selected samples along the New Zealand transect, and across the Drake Passage show: (a) differences
339 in calcification among the various *E. huxleyi* morphotypes, being very evident in type A (Figs. 3 b-c, 4 b-c, 5, and 7), (b) a
340 wide scatter of relative tube width' within morphotypes and within each sample, especially marked in the New Zealand transect
341 (Figs. 4b, 7) and (c) a slight decreasing trend in coccolith size and degree of calcification across the Drake Passage (Figs. 3b,
342 5a), which is not observed in the New Zealand transect. This suggests that environmental forcing does not significantly impact
343 the degree of calcification but it clearly controls the distribution of *E. huxleyi* morphotypes (which are genetically-based,
344 Bendif et al., 2023) and thus indirectly impacts on the coccolith mass variation. This could also explain the southwards
345 decreasing trend in calcification in the Drake Passage due to the fact that the relatively large and heavily calcified type A
346 coccospheres are present in the northern SAZ. The PCA performed on the *E. huxleyi* morphometric dataset shows that those
347 heavily calcified type A coccospheres occupy a relatively restricted ecological niche offshore of Chile (Fig. 7).

348
349 In general, we find a different pattern than Balch et al. (2014), who determined coccolith-quotas in the center of a
350 coccolithophore bloom in the Patagonian Shelf (Atlantic Ocean) ranging from 0.008 to 0.017 pg per coccolith by comparing
351 automated coccolith-counts with in-situ PIC. In the context of other observations, the coccolith quotas calculated by Balch et



352 al. (2014) are relatively low and show a much greater variation within a limited region. Given the above evidence in two
353 different transects of the SO and sampling 11 years apart, we assume that with our approach, our coccolith-PIC calculations
354 do not underestimate actual sea surface PIC concentration. We attribute the discrepancy between the coccolithophore in-situ
355 and satellite-derived PIC to overestimation of the algorithm in the SO, due to the limited number of data points used for the
356 calibration.

357 **5.2 Assessing potential biases in PIC estimates for the AZ**

358 In the AZ (south of about 62.5°S in the New Zealand transect and about 60°S in the Drake Passage), high reflectance is detected
359 by remote sensing but it is not associated with a coccolithophore bloom (Figs. 3 and 4). Concentration of *E. huxleyi*, which
360 show maximum numbers in the PFZ at the New Zealand transect and moderate values in the Drake Passage, drops southward
361 of this location (Malinverno et al., 2016), at the Southern ACC Front and the PF.

362
363 Satellite data show the different impact of ACC fronts on the distribution of *E. huxleyi* (Holligan et al., 2010): in the Drake
364 Passage, where the fronts are strictly constrained by topography, *E. huxleyi* is bounded by the PF to the south (Saavedra-
365 Pellitero et al., 2019), while in the eastern Scotia Sea, where the ACC fronts are broadly separated, *E. huxleyi* spreads between
366 the PF and the Southern ACC Front (Holligan et al., 2010; Poulton et al., 2011; Poulton et al., 2013). This pattern also emerges
367 from the compilation by Malinverno et al. (2016), which shows that the Southern ACC Front marks the southern boundary in
368 different ocean sectors.

369
370 Occasional occurrences of *E. huxleyi* south of the Southern ACC Front have been documented south of Tasmania and in the
371 Weddell sea in certain years by conventional micropalaeontological observations (e.g. Winter et al., 1999; Cubillos et al.,
372 2007) as well as in the Australian sector of the SO and in the Scotia Sea using surface reflectance data only (Holligan et al.,
373 2010; Winter et al., 2014). However, in the present work, *E. huxleyi* is constrained by the Southern ACC Front corresponding
374 to a sea surface temperature of 1°C in the New Zealand transect.

375
376 The magnitude and spectral characteristics of water-leaving radiance detected by satellites are influenced by the inherent
377 properties of the optically active constituents. These include: (1) light scattering by PIC, other biogenic particles or lithogenic
378 material (e.g. Bi et al., 2023) as well as (2) light absorption by phytoplankton biomass (i.e., chlorophyll-a concentration) and
379 dissolved organic matter (e.g. Reynolds et al., 2001; Ferreira et al., 2009). The strong correlation between high values of water-
380 leaving radiance and high *E. huxleyi* PIC concentrations has been successfully proved in bloom areas (e.g. Gordon et al., 1988;
381 Balch et al., 2005; Holligan et al., 2010; Balch et al., 2011; Balch et al., 2014; Balch and Mitchell, 2023; Oliver et al., in press).
382 However, not all bright waters are caused by *E. huxleyi* blooms, as shown by Broerse et al. (2003) in the Bering Sea, Balch et
383 al. (2007) in the Gulf of Maine, and Daniels et al. (2012) in the Bay of Biscay. Suspended particles, which include either



384 reworked coccoliths, lithogenic material or empty diatom frustules, could be responsible for high values of water-leaving
385 radiance, at least in nearshore regions (Broerse et al., 2003; Balch and Mitchell, 2023).

386

387 The occurrence of bright waters along the studied transects should theoretically be constrained by the position of the PF/
388 Southern ACC Front. Malinverno et al. (2015; 2016) showed a significant shift in the community composition from carbonate
389 to silica-dominated microfossils in the New Zealand transect at the Southern ACC Front. Coccolithophores disappear south of
390 the Southern ACC Front, and the composition of the siliceous phytoplankton changes from a dominance of large diatoms
391 (*Fragilariopsis kerguelensis*) in the north to a dominance of small diatoms (such as the cold adapted *Fragilariopsis cylindrus*)
392 in the south, with a notable increase in spiny silicoflagellates (e.g., *Stephanocha speculum* var. *coronata*) and small siliceous
393 plankton (Parnales, Archaeomonads) (Malinverno et al., 2016) (Fig. 9). The diatoms present have not yet been studied in the
394 exact same water samples collected during PS97 Expedition. However, the abundance of subfossil diatoms in surface
395 sediments in the Drake Passage shows an increase south of the PF, along with an increase in the relative abundance of
396 siliciclastics and in biogenic opal (Cárdenas et al., 2018). *Fragilariopsis kerguelensis* appears to dominate up to the Southern
397 ACC Front, and *F. cylindrus* is found south of this front, in colder waters of the Drake Passage (Cárdenas et al., 2018). Although
398 opal particles have a much lower refractive index than calcite (Balch, 2009; Costello et al., 1995), we suggest that the high
399 abundance of small opal particles observed could explain the observed high scattering of these waters at least in the New
400 Zealand transect (Figs. 1, 3, 4). Alternative sources of high reflectance in the SO considered by other authors include
401 microbubbles (mostly during storms), floating loose ice or high concentrations of other particulate matter such as glacial flour
402 (especially close to the Antarctic continent) or *Phaeocystis* blooms (Balch et al., 2011; Balch, 2018; Balch and Mitchell, 2023).

403 **5.3 *Emiliana huxleyi* morphotypes**

404 The PCA performed on the *E. huxleyi* morphometric dataset in particular reveals a Type A overcalcified morphotype that is
405 highly distinct from the other morphotypes (Fig. 6). This morphotype has also been previously observed in the coastal waters
406 of the eastern South Pacific and in the open ocean (Beaufort et al., 2011; Von Dassow et al., 2018; Saavedra-Pellitero et al.,
407 2019). However, it should be noted that type A overcalcified in this work includes the moderately calcified, robustly calcified
408 and extremely heavily calcified A morphotypes described by Diaz-Rosas et al. (2021). Coccospheres of *E. huxleyi* classified
409 by Diaz-Rosas et al. (2021) as extremely heavily calcified R/hyper-calcified and/or A-CC morphotypes (with complete
410 overgrowth of the coccolith central area but without fusion of distal shield elements) occasionally occurred offshore of Chile
411 in samples closest to the coastline (see an example in Figure 6). In the Southern Hemisphere, these extremely heavily calcified
412 morphotypes were only previously observed at the Pacific border of southern Patagonia (in the Archipelago Madre de Dios
413 Fjord area) and in the Northern Hemisphere, in Norwegian fjords (e.g. Young et al., 2014). Diaz-Rosas et al. (2021) suggested
414 that the R/hyper-calcified morphotype has a marginal ecological niche preference compared to moderately calcified types A
415 and A-CC. Therefore the few specimens of *E. huxleyi* type A overcalcified (i.e. heavily calcified looking in between the



416 R/hyper-calcified and/or A-CC morphotypes by Diaz-Rosas et al. (2021)) observed in this work, and by Saavedra-Pellitero et
417 al. (2019) in the Drake Passage, could be attributed to different niches overlapping offshore of Chile.

418
419 The normal type A specimens show a moderate range of variation in tube width, comparable to type O, but smaller than B,
420 B/C-C, with type C having the thinnest tube width. The distal shield element width and the number of T-elements of the
421 different specimens are closely related to the length and width measured (Fig. 7) as they are all indicators of coccolith size.
422 There is broader variation in coccolith size (length and width) within morphogroup B compared to morphogroup A, which is
423 more restricted. Suchéras-Marx et al (2022) pointed out that *E. huxleyi* coccolith size is limited by the cell diameter because
424 heterococcoliths are produced intracellularly and are extruded later on. Interestingly, specimens of *E. huxleyi* type A in the
425 New Zealand transect are notably smaller than those offshore of Chile, which we link to local adaptations, seasonality and
426 even ecological interactions such as predation (e.g. Monteiro et al., 2016; Hansen et al., 1996).

427
428 However, the coccolithophore assemblages in the PFZ and south of it are monospecific, which is also known from other areas
429 of the SO (e.g. Charalampopoulou et al., 2016), and consist almost entirely of *E. huxleyi* morphogroup B. The mean placolith
430 length of *E. huxleyi* morphogroup B (including types B, B/C-C, and O) in both transects is very similar (Drake Passage: 2.98
431 μm , New Zealand: 2.87 μm) and agrees well with the corresponding B/C measurements of Charalampopoulou et al. (2016) in
432 samples retrieved in 2009 in the Drake Passage (2.8 μm). Still, our averaged values are slightly lower than the mean length
433 estimated by Poulton et al. (2011) on the Patagonian Shelf (3.25 \pm 0.40 μm). This could be due to the fact that Poulton et al.
434 (2011) did not distinguish between types B and O (i.e. they were merged into B/C), which are typically larger coccoliths than
435 B/C (Fig. 6) and could have contributed to increase the averaged length. The length range for types B/C-C (Drake Passage:
436 2.2 to 3.98 μm , New Zealand: 1.95 to 3.62 μm) agrees quite well with the range reported by Cook et al. (2011) for cultured
437 B/C strains (2.65 to 4.80 μm) and is in the range of sizes presented by Charalampopoulou et al. (2016) for the Drake Passage
438 (1.8 to 5.5 μm). The fact that we record lower values is simply a matter of taxonomical considerations regarding the overlapping
439 morphotypes B, B/C, C and O, visually represented in Figure 6.

440
441 The different taxonomic considerations of *E. huxleyi* by various studies make it difficult to compare and combine data,
442 especially in light of recent advances in the field. Given the dominance of this taxa in the SO, a key area for global warming
443 and ocean acidification studies, the efforts of the scientific nannofloral community should focus on a more uniform
444 classification of *E. huxleyi* morphotypes. However, differentiation and recognition of the various morphotypes plays only a
445 minor role in the calculation of the total coccolithophorid PIC, as observed in other areas of the SO (e.g. Rigual Hernández et
446 al., 2020a, b). The changes in masses within the B morphotype (with types B/C-C, C, O) in the two transects are negligible in
447 the PIC calculation, while a differentiation into morphogroups A and B has an influence on the calculation of the PIC. However,
448 specimens of *E. huxleyi* belonging to morphogroup A only occur in the northern areas of both transects, where they play a role
449 together with the PIC input from other massive species such as *C. leptoporus* (Fig. 5). Overall, the changes in total coccolith-



450 PIC in the study area are caused by the abundance and occurrence within the entire coccolithophore community. The relative
451 contribution of the different *E. huxleyi* morphogroups to the coccolith-PIC in the SO deserves further exploration in light of
452 the rapid development of remote sensing algorithms and recent evolution of machine learning approaches for PIC estimates.

453 **6 Conclusions/Summary**

454 The comparison between particulate inorganic carbon (PIC) derived from satellite data and in situ coccolithophore-based
455 estimates in two transects of the Pacific sector (separated in time and space) provides an invaluable ground truth benchmark
456 for the study of coccolithophores at high latitudes. Based on our data the following conclusions can be drawn:

457

458 1) We found out that satellite-derived PIC values and coccolith-PIC trends are in good agreement in the Subantarctic
459 Zone (SAZ) and Polar Front Zone (PFZ). However, remote sensing tends to overestimate PIC values, which we link
460 to a certain bias in the algorithm due to the limited number of measurements used for the validation of the PIC
461 calibration (all of them in the Atlantic ocean). This could be potentially adjusted for in the Southern Ocean and
462 specifically for the study area.

463

464 2) A striking observation is the decoupling of satellite-derived PIC and coccolith-PIC estimates at and to the south of
465 the Polar Front (PF), particularly in the Antarctic Zone (AZ). Despite having high reflectance values, no
466 coccolithophores were observed in this area. We hypothesize that the high satellite-derived PIC values in the AZ
467 could be due to the high abundance of small opal particles.

468

469 3) *Emiliana huxleyi* is the predominant coccolithophore species contributing the most to the sea-surface PIC in the New
470 Zealand transect (mainly sampled in 2005) and as well as in the Drake Passage (sampled in 2016). *Calcidiscus*
471 *leptoporus* may occasionally contribute significantly to the PIC contributions at certain locations, whereas the rest of
472 the coccolithophore taxa contribute only marginally to the PIC in the studied areas.

473

474 4) *Emiliana huxleyi* consists of different morphotypes, which have different, partly overlapping geographical
475 distributions. The relatively massive Type A occurs in the northern SAZ and occasionally in the PFZ of the Drake
476 Passage, while specimens of the less calcified morphogroup B (which includes Types B, B/C, C and O) occur in the
477 SAZ and the PFZ of both transects, but disappear drastically south of the PF. But neither the slightly different
478 carbonate masses nor the southward changes in morphotype composition have a decisive influence on the
479 coccolithophore-derived PIC, which is only determined by the amount of *E. huxleyi* in this area.

480



481 5) The satellite-derived and coccolith-PIC discrepancy we observed in this work emphasizes the importance of in situ
482 measurements and highlights the need for further investigation to fully understand the factors influencing water-
483 leaving radiance and the reliability of remote sensing estimates, especially south of the PF.

484

485 Future research should focus on refining satellite algorithms to improve the accuracy of PIC estimates and better understand
486 the dynamics of coccolithophore communities in the Pacific sector of the Southern Ocean (especially compared to the Atlantic
487 and Indian sectors). Such efforts will enhance our understanding of carbon cycling and its impact on marine ecosystems in this
488 key high latitude region.

489 **Acknowledgements**

490 The Particulate Inorganic Carbon (PIC) data were downloaded from the OceanColor Web Level-3 & 4 Browser
491 (<https://oceancolor.gsfc.nasa.gov/l3>), a service provided by NASA's Ocean Biology Distributed Active Archive Centre.

492 The authors acknowledge the use of the JASMIN (Joint Analysis System for the Met Office, NERC, and UKRI) Jupyter
493 Notebook service to process the PIC data. We would like to express our gratitude to the JASMIN team for their support and
494 the valuable resources they provide to the scientific community.

495 The Alfred Wegener Institute Bremerhaven provided part of the plankton samples required for this study. Frank Lamy, Hartmut
496 Schulz, R/V POLARSTERN officers and crew are thanked for their help during the PS97 Expedition.

497 Dr. Frigola (Barcelona Supercomputing Center, Spain), Dr. Merkel (University of Bremen/MARUM, Germany) and Dr.
498 Hardiman (University of Portsmouth, UK) are acknowledged for their help with remote sensing data collection. Dr. Pepin
499 (University of Portsmouth, UK) and Dr. Balch (Bigelow Laboratory for Ocean Sciences, USA) are thanked for their comments
500 and suggestions on this piece of research during the "Advances in Coccolithophore research" meeting. Dr. Saavedra (RIP) is
501 thanked for his continuous encouragement to finish up this paper.

502 **Financial support**

503 This research was supported by University of Portsmouth Open Access Fund. The Deutsche Forschungsgemeinschaft grant
504 Adaptation of coccolithophore communities to environmental change in the Southern Ocean (no. BA 1648/30-1) to Karl-Heinz
505 Baumann contributed with previous funding for Mariem Saavedra-Pellitero and Nele M. Vollmar and the MIUR project
506 "Dipartimenti di Eccellenza 2018/2023" for Elisa Malinverno, at Department of Earth and Environmental Sciences, University
507 of Milano-Bicocca.

508

509 **Data Availability Statement**



510 The authors confirm that the data from which the findings of this study are available within the article Supplementary Materials
511 and are stored in the data repository <https://pangaea.de/>

512

513 **Author contributions**

514 The study was designed by EM, MSP and KHB. EM and NMV carried out the morphometric measurements and classified the
515 specimens of *E. huxleyi*. EM and MSP calculated coccolith-PICs, plotted the data and wrote an earlier version of the
516 manuscript. N B-J and HL provided remote sensing data for the study area, and were actively involved in the discussion of the
517 findings as well as in the writing of the paper. All authors approved the submitted version.

518 **References**

- 519 Babin, M., Morel, A., Fournier-Sicre, V., Fell, F., and Stramski, D.: Light scattering properties of marine particles in coastal
520 and open ocean waters as related to the particle mass concentration, *Limnology and Oceanography*, 48, 843-859, doi:
521 10.4319/lo.2003.48.2.0843, 2003a.
- 522 Babin, M., Stramski, D., Ferrari, G. M., Claustre, H., Bricaud, A., Obolensky, G., and Hoepffner, N.: Variations in the light
523 absorption coefficients of phytoplankton, nonalgal particles, and dissolved organic matter in coastal waters around
524 Europe, *Journal of Geophysical Research: Oceans*, 108, doi: 10.1029/2001JC000882, 2003b.
- 525 Balch, W. M.: The Ecology, Biogeochemistry, and Optical Properties of Coccolithophores, *Annual Review of Marine Science*,
526 10, 71-98, doi: 10.1146/annurev-marine-121916-063319, 2018.
- 527 Balch, W. M., Holligan, P. M., Ackleson, S. G., and Voss, K. J.: Biological and optical properties of mesoscale coccolithophore
528 blooms in the Gulf of Maine, *Limnology and Oceanography*, 36, 629-643, doi: 10.4319/lo.1991.36.4.0629, 1991.
- 529 Balch, W. M., Kilpatrick, K. A., Holligan, P., Harbour, D., and Fernandez, E.: The 1991 coccolithophore bloom in the central
530 North Atlantic. 2. Relating optics to coccolith concentration, *Limnology and Oceanography*, 41, 1684-1696, 1996.
- 531 Balch, W. M., Drapeau, D. T., Cucci, T. L., Vaillancourt, R. D., Kilpatrick, K. A., and Fritz, J. J.: Optical backscattering by
532 calcifying algae: Separating the contribution of particulate inorganic and organic carbon fractions, *Journal of Geophysical
533 Research: Oceans*, 104, 1541-1558, doi: 10.1029/1998JC900035, 1999.
- 534 Balch, W. M., Gordon, H. R., Bowler, B. C., Drapeau, D. T., and Booth, E. S.: Calcium carbonate measurements in the surface
535 global ocean based on Moderate-Resolution Imaging Spectroradiometer data, *Journal of Geophysical Research: Oceans*,
536 110, doi: 10.1029/2004JC002560, 2005.
- 537 Balch, W. M., Drapeau, D. T., Bowler, B. C., Booth, E. S., Windecker, L. A., and Ashe, A.: Space-time variability of carbon
538 standing stocks and fixation rates in the Gulf of Maine, along the GNATS transect between Portland, ME, USA, and
539 Yarmouth, Nova Scotia, Canada, *Journal of Plankton Research*, 30, 119-139, doi: 10.1093/plankt/fbm097, 2007.
- 540 Balch, W. M., Drapeau, D. T., Bowler, B. C., Lyczkowski, E., Booth, E. S., and Alley, D.: The contribution of
541 coccolithophores to the optical and inorganic carbon budgets during the Southern Ocean Gas Exchange Experiment: New



- 542 evidence in support of the “Great Calcite Belt” hypothesis, *Journal of Geophysical Research: Oceans*, 116, doi:
543 10.1029/2011jc006941, 2011.
- 544 Balch, W. M., Drapeau, D. T., Bowler, B. C., Lyczkowski, E. R., Lubelczyk, L. C., Painter, S. C., and Poulton, A. J.: Surface
545 biological, chemical, and optical properties of the Patagonian Shelf coccolithophore bloom, the brightest waters of the
546 Great Calcite Belt, *Limnology and Oceanography*, 59, 1715-1732, doi: 10.4319/lo.2014.59.5.1715, 2014.
- 547 Balch, W. M., Bates, N. R., Lam, P. J., Twining, B. S., Rosengard, S. Z., Bowler, B. C., Drapeau, D. T., Garley, R., Lubelczyk,
548 L. C., Mitchell, C., and Rauschenberg, S.: Factors regulating the Great Calcite Belt in the Southern Ocean and its
549 biogeochemical significance, *Global Biogeochemical Cycles*, 30, 1124-1144, doi: 10.1002/2016gb005414, 2016.
- 550 Balch, W. M., and Mitchell, C.: Remote sensing algorithms for particulate inorganic carbon (PIC) and the global cycle of PIC,
551 *Earth-Science Reviews*, 239, 104363, doi: 10.1016/j.earscirev.2023.104363, 2023.
- 552 Balch, W. M., and P.E. Utgoff: Potential interactions among ocean acidification, coccolithophores, and the optical properties
553 of seawater, *Oceanography and Marine Biology Annual Review*, 22, 146-159, doi: 10.5670/oceanog.2009.104, 2009.
- 554 Beaufort, L.: Weight estimates of coccoliths using the optical properties (birefringence) of calcite, *Micropaleontology*, 51,
555 289–298, 2005.
- 556 Beaufort, L., Probert, I., de Garidel-Thoron, T., Bendif, E. M., Ruiz-Pino, D., Metzl, N., Goyet, C., Buchet, N., Coupel, P.,
557 Grelaud, M., Rost, B., Rickaby, R. E. M., and de Vargas, C.: Sensitivity of coccolithophores to carbonate chemistry and
558 ocean acidification, *Nature*, 476, 80-83, doi: 10.1038/nature10295, 2011.
- 559 Bendif, E. M., Probert, I., Archontikis, O. A., Young, J. R., Beaufort, L., Rickaby, R. E., and Filatov, D.: Rapid diversification
560 underlying the global dominance of a cosmopolitan phytoplankton, *The ISME Journal*, 17, 630-640, doi: 10.1038/s41396-
561 023-01365-5, 2023.
- 562 Beuvier, T., Probert, I., Beaufort, L., Suchéras-Marx, B., Chushkin, Y., Zontone, F., and Gibaud, A.: X-ray nanotomography
563 of coccolithophores reveals that coccolith mass and segment number correlate with grid size, *Nature Communications*,
564 10, 751, doi: 10.1038/s41467-019-08635-x, 2019.
- 565 Bi, S., Hieronymi, M., and Röttgers, R.: Bio-geo-optical modelling of natural waters, *Frontiers in Marine Science*, 10, doi:
566 10.3389/fmars.2023.1196352, 2023.
- 567 Bollmann, J.: Technical Note: Weight approximation of coccoliths using a circular polarizer and interference colour derived
568 retardation estimates - (The CPR Method), *Biogeosciences*, 11, 1899-1910, doi: 10.5194/bg-11-1899-2014, 2014.
- 569 Broerse, A. T. C., Tyrrell, T., Young, J. R., Poulton, A. J., Merico, A., Balch, W. M., and Miller, P. I.: The cause of bright
570 waters in the Bering Sea in winter, *Continental Shelf Research*, 23, 1579-1596, doi: 10.1016/j.csr.2003.07.001, 2003.
- 571 Cárdenas, P., Lange, C. B., Vernet, M., Esper, O., Srain, B., Vorrath, M.-E., Ehrhardt, S., Müller, J., Kuhn, G., Arz, H. W.,
572 Lembke-Jene, L., and Lamy, F.: Biogeochemical proxies and diatoms in surface sediments across the Drake Passage
573 reflect oceanic domains and frontal systems in the region, *Progress in Oceanography*, doi: 10.1016/j.pocean.2018.10.004,
574 2018.



- 575 Charalampopoulou, A., Poulton, A. J., Bakker, D. C. E., Lucas, M. I., Stinchcombe, M. C., and Tyrrell, T.: Environmental
576 drivers of coccolithophore abundance and calcification across Drake Passage (Southern Ocean), *Biogeosciences*, 13,
577 5917-5935, doi:10.5194/bg-13-5917-2016, 2016.
- 578 Cook, S. S., Whittock, L., Wright, S. W., and Hallegraeff, G. M.: Photosynthetic pigment and genetic differences between two
579 Southern Ocean morphotypes of *Emiliana huxleyi* (Haptophyta), *Journal of Phycology*, 47, 615-626, doi:
580 10.1111/j.1529-8817.2011.00992.x, 2011.
- 581 Costello, D. K., Carder, K. L., and Hou, W.: Aggregation of diatom bloom in a mesocosm: Bulk and individual particle optical
582 measurements, *Deep Sea Research Part II: Topical Studies in Oceanography*, 42, 29-45, doi: 10.1016/0967-
583 0645(95)00003-9, 1995.
- 584 Cros, L., Kleijne, A., Zeltner, A., Billard, C., and Young, J. R.: New examples of holococcolith-heterococcolith combination
585 coccospheres and their implications for coccolithophorid biology, *Marine Micropaleontology*, 39, 1-34, doi:
586 10.1016/S0377-8398(00)00010-4, 2000.
- 587 Cubillos, J. C., Wright, S. W., Nash, G., de Salas, M. F., Griffiths, B., Tilbrook, B., Poisson, A., and Hallegraeff, G. M.:
588 Calcification morphotypes of the coccolithophorid *Emiliana huxleyi* in the Southern Ocean: changes in 2001 to 2006
589 compared to historical data, *Marine Ecology Progress Series*, 348, 47-54, doi: 10.3354/meps07058, 2007.
- 590 Daniels, C. J., Tyrrell, T., Poulton, A. J., and Pettit, L.: The influence of lithogenic material on particulate inorganic carbon
591 measurements of coccolithophores in the Bay of Biscay, *Limnology and Oceanography*, 57, 145-153, doi:
592 10.4319/lo.2012.57.1.0145, 2012.
- 593 Davis, J. C.: *Statistics and Data Analysis in Geology*, John Wiley & Sons, 1986.
- 594 de Baar, H. J. W., de Jong, J. T. M., Bakker, D. C. E., Loscher, B. M., Veth, C., Bathmann, U., and Smetacek, V.: Importance
595 of iron for plankton blooms and carbon dioxide drawdown in the Southern Ocean, *Nature*, 373, 412-415, doi:
596 10.1038/373412a0, 1995.
- 597 Devred, E., Sathyendranath, S., Stuart, V., Maass, H., Ulloa, O., and Platt, T.: A two-component model of phytoplankton
598 absorption in the open ocean: Theory and applications, *Journal of Geophysical Research: Oceans*, 111, doi:
599 10.1029/2005JC002880, 2006.
- 600 Díaz-Rosas, F., Alves-de-Souza, C., Alarcón, E., Menschel, E., González, H. E., Torres, R., and von Dassow, P.: Abundances
601 and morphotypes of the coccolithophore *Emiliana huxleyi* in southern Patagonia compared to neighbouring oceans and
602 Northern Hemisphere fjords, *Biogeosciences*, 18, 5465-5489, doi: 10.5194/bg-18-5465-2021, 2021.
- 603 Ferreira, A., Garcia, V. M. T., and Garcia, C. A. E.: Light absorption by phytoplankton, non-algal particles and dissolved
604 organic matter at the Patagonia shelf-break in spring and summer, *Deep Sea Research Part I: Oceanographic Research
605 Papers*, 56, 2162-2174, doi: 10.1016/j.dsr.2009.08.002, 2009.
- 606 Fuertes, M.-Á., Flores, J.-A., and Sierro, F. J.: The use of circularly polarized light for biometry, identification and estimation
607 of mass of coccoliths, *Marine Micropaleontology*, 113, 44-55, doi: 10.1016/j.marmicro.2014.08.007, 2014.



- 608 GEBCO Compilation Group: GEBCO_2022 Grid. Data set available online from the British Oceanographic Data Centre,
609 Liverpool, UK. doi: 10.5285/e0f0bb80-ab44-2739-e053-6c86abc0289c, 2022.
- 610 Gordon, A. L., Molinelli, E., and Baker, T.: Large-scale relative dynamic topography of the Southern Ocean, *Journal of*
611 *Geophysical Research: Oceans*, 83, 3023-3032, doi: 10.1029/JC083iC06p03023, 1978.
- 612 Gordon, H. R., Brown, O. B., Evans, R. H., Brown, J. W., Smith, R. C., Baker, K. S., and Clark, D. K.: A semianalytic radiance
613 model of ocean color, *Journal of Geophysical Research: Atmospheres*, 93, 10909-10924, doi:
614 10.1029/JD093iD09p10909, 1988.
- 615 Gordon, H. R., Boynton, G. C., Balch, W. M., Groom, S. B., Harbour, D. S., and Smyth, T. J.: Retrieval of coccolithophore
616 calcite concentration from SeaWiFS Imagery, *Geophysical Research Letters*, 28, 1587-1590, doi:
617 10.1029/2000GL012025, 2001.
- 618 Gravalosa, J. M., Flores, J.-A., Sierro, F. J., and Gersonde, R.: Sea surface distribution of coccolithophores in the eastern
619 Pacific sector of the Southern Ocean (Bellingshausen and Amundsen Seas) during the late austral summer of 2001,
620 *Marine Micropaleontology*, 69, 16-25, doi: 10.1016/j.marmicro.2007.11.006, 2008.
- 621 Guitián, J., Fuertes, M. Á., Flores, J. A., Hernández-Almeida, I., and Stoll, H.: Variation in calcification of *Reticulofenestra*
622 coccoliths over the Oligocene–Early Miocene, *Biogeosciences*, 19, 5007-5019, doi: 10.5194/bg-19-5007-2022, 2022.
- 623 Oliver, H., McGillicuddy, D. J., J., Krumhardt, K. M., Long, M. C., Bates, N. R., Bowler, B. C., Drapeau, D. T., and Balch,
624 W. M.: Environmental drivers of coccolithophore growth in the Pacific sector of the Southern Ocean, *Global*
625 *Biogeochemical Cycles*, in press.
- 626 Hammer, Ø., Harper, D. A. T., and Ryan, P. D.: PAST: paleontological Statistics software package for education and data
627 analysis, *Paleontologia Electronica*, 49, 9, 2001.
- 628 Hansen, F. C., Witte, H. J., and Passarge, J.: Grazing in the heterotrophic dinoflagellate *Oxyrrhis marina*: Size selectivity and
629 preference for calcified *Emiliania huxleyi* cells., *Aquatic Microbial Biology*, 10, 307–313, 1996.
- 630 Harlay, J., Borges, A. V., Van Der Zee, C., Delille, B., Godoi, R. H. M., Schiettecatte, L. S., Roevros, N., Aerts, K., Lapernat,
631 P. E., Rebreanu, L., Groom, S., Daro, M. H., Van Grieken, R., and Chou, L.: Biogeochemical study of a coccolithophore
632 bloom in the northern Bay of Biscay (NE Atlantic Ocean) in June 2004, *Progress in Oceanography*, 86, 317-336, doi:
633 10.1016/j.pocean.2010.04.029, 2010.
- 634 Harper, D. A. T.: *Numerical Palaeobiology*, John Wiley & Sons, 1999.
- 635 Holligan, P. M., Viollier, M., Harbour, D. S., Camus, P., and Champagne-Philippe, M.: Satellite and ship studies of
636 coccolithophore production along a continental shelf edge, *Nature*, 304, 339-342, doi: 10.1038/304339a0, 1983.
- 637 Holligan, P. M., Charalampopoulou, A., and Hutson, R.: Seasonal distributions of the coccolithophore, *Emiliania huxleyi*, and
638 of particulate inorganic carbon in surface waters of the Scotia Sea, *Journal of Marine Systems*, 82, 195-205, doi:
639 10.1016/j.jmarsys.2010.05.007, 2010.
- 640 Horigome, M. T., Ziveri, P., Grelaud, M., Baumann, K. H., Marino, G., and Mortyn, P. G.: Environmental controls on the
641 *Emiliania huxleyi* calcite mass, *Biogeosciences*, 11, 2295-2308, doi: 10.5194/bg-11-2295-2014, 2014.



- 642 Iida, T., Saitoh, S. I., Miyamura, T., Toratani, M., Fukushima, H., and Shiga, N.: Temporal and spatial variability of
643 coccolithophore blooms in the eastern Bering Sea, 1998-2001, *Progress in Oceanography*, 55, 165-175, doi:
644 10.1016/S0079-6611(02)00076-9, 2002.
- 645 Kleijne, A.: Morphology, taxonomy and distribution of extant coccolithophores (calcareous nanoplankton), Ph.D., Vrije
646 Universiteit, Amsterdam, 321 pp., 1993.
- 647 Klinck, J., and Nowlin, W. D.: Antarctic Circumpolar Current, in: *Encyclopedia of Ocean Sciences*, edited by: Steele, J. H.,
648 Academic Press, Oxford, 151-159, 2001.
- 649 Krumhardt, K. M., Lovenduski, N. S., Long, M. C., Levy, M., Lindsay, K., Moore, J. K., and Nissen, C.: Coccolithophore
650 growth and calcification in an acidified ocean: Insights from Community Earth System Model simulations, *Journal of*
651 *Advances in Modeling Earth Systems*, doi: 10.1029/2018ms001483, 2019.
- 652 Lamy, F.: The Expedition PS97 of the Research Vessel POLARSTERN to the Drake Passage in 2016, edited by: *Berichte zur*
653 *Polar- und Meeresforschung = Reports on polar and marine research*, E. b. F. L. w. c. o. t. p., 167 pp., 2016.
- 654 Legendre, P., and Legendre, L.: *Numerical Ecology*, 2nd ed., Elsevier, 1998.
- 655 Malinverno, E., Triantaphyllou, M. V., and Dimiza, M. D.: Coccolithophore assemblage distribution along a temperate to polar
656 gradient in the West Pacific sector of the Southern Ocean (January 2005) *Micropaleontology*, 61, 489-506 2015.
- 657 Malinverno, E., Maffioli, P., and Gariboldi, K.: Latitudinal distribution of extant fossilizable phytoplankton in the Southern
658 Ocean: Planktonic provinces, hydrographic fronts and palaeoecological perspectives, *Marine Micropaleontology*, 123,
659 41-58, doi: 10.1016/j.marmicro.2016.01.001, 2016.
- 660 Mitchell, C., Hu, C., Bowler, B., Drapeau, D., and Balch, W. M.: Estimating Particulate Inorganic Carbon Concentrations of
661 the Global Ocean From Ocean Color Measurements Using a Reflectance Difference Approach, *Journal of Geophysical*
662 *Research: Oceans*, 122, 8707-8720, doi: 10.1002/2017JC013146, 2017.
- 663 Mohan, R., Mergulhao, L. P., Guptha, M. V. S., Rajakumar, A., Thamban, M., AnilKumar, N., Sudhakar, M., and Ravindra,
664 R.: Ecology of coccolithophores in the Indian sector of the Southern Ocean, *Marine Micropaleontology*, 67, 30-45, doi:
665 10.1016/j.marmicro.2007.08.005, 2008.
- 666 Monteiro, F. M., Bach, L. T., Brownlee, C., Bown, P., Rickaby, R. E. M., Poulton, A. J., Tyrrell, T., Beaufort, L., Dutkiewicz,
667 S., Gibbs, S., Gutowska, M. A., Lee, R., Riebesell, U., Young, J., and Ridgwell, A.: Why marine phytoplankton calcify,
668 *Science Advances*, 2, e1501822, doi: doi:10.1126/sciadv.1501822, 2016.
- 669 NASA Ocean Biology Processing Group: Using the Level 3 Browser Interface. Available from
670 <https://oceancolor.gsfc.nasa.gov/l3/help/>, 2018 [Access 14 June 2023].
- 671 NASA Goddard Space Flight Center, Ocean Ecology Laboratory, Ocean Biology Processing Group: Moderate-resolution
672 Imaging Spectroradiometer (MODIS) Aqua Level-3 Mapped Particulate Inorganic Carbon, Version 2022 Data; NASA
673 OB.DAAC, Greenbelt, MD, USA. doi: 10.5067/AQUA/MODIS/L3M/PIC/2022, 2022 [Access 01 June 2023].
- 674 NASA Ocean Biology Processing Group: Particulate Inorganic Carbon (PIC). Available from
675 <https://oceancolor.gsfc.nasa.gov/resources/atbd/pic/>, 2023a [Access 14 June 2023].



- 676 NASA Ocean Biology Processing Group: Ocean Color Reprocessing 2022.0. Available from
677 <https://oceancolor.gsfc.nasa.gov/data/reprocessing/r2022/>, 2023b [Access 14 June 2023].
- 678 NASA Ocean Biology Processing Group: MODIS/Aqua Ocean Color Reprocessing 2022.0. Available from
679 <https://oceancolor.gsfc.nasa.gov/data/reprocessing/r2022/aqua/>, 2023c. [Access 14 June 2023].
- 680 Neukermans, G., Oziel, L., and Babin, M.: Increased intrusion of warming Atlantic water leads to rapid expansion of temperate
681 phytoplankton in the Arctic, *Global Change Biology*, 24, 2545-2553, doi: 10.1111/gcb.14075, 2018.
- 682 Okada, H., and McIntyre, A.: Modern coccolithophores of the Pacific and North Atlantic oceans, *Micropaleontology*, 23, 1-
683 54, doi: 10.2307/1485309 1977.
- 684 Orsi, A. H., and Harris, U.: Fronts of the Antarctic Circumpolar Current - GIS data, Ver. 1, Australian Antarctic Data Centre
685 - https://data.aad.gov.au/metadata/records/antarctic_circumpolar_current_fronts, 2019 [Access 26 May 2023].
- 686 Orsi, A. H., Whitworth III, T., and Nowlin Jr, W. D.: On the meridional extent and fronts of the Antarctic Circumpolar Current,
687 *Deep Sea Research Part I: Oceanographic Research Papers*, 42, 641-673, doi: 10.1016/0967-0637(95)00021-w, 1995.
- 688 Poulton, A. J., Young, J. R., Bates, N. R., and Balch, W. M.: Biometry of detached *Emiliana huxleyi* coccoliths along the
689 Patagonian Shelf, *Marine Ecology Progress Series*, 443, 1-17, doi: 10.3354/meps09445, 2011.
- 690 Poulton, A. J., Painter, S. C., Young, J. R., Bates, N. R., Bowler, B., Drapeau, D., Lyczszkowski, E., and Balch, W. M.: The
691 2008 *Emiliana huxleyi* bloom along the Patagonian Shelf: Ecology, biogeochemistry, and cellular calcification, *Global
692 Biogeochemical Cycles*, 27, 1023-1033, doi: 10.1002/2013GB004641, 2013.
- 693 Reynolds, R. A., Stramski, D., and Mitchell, B. G.: A chlorophyll-dependent semianalytical reflectance model derived from
694 field measurements of absorption and backscattering coefficients within the Southern Ocean, *Journal of Geophysical
695 Research: Oceans*, 106, 7125-7138, doi: 10.1029/1999JC000311, 2001.
- 696 Rigual Hernández, A. S., Flores, J. A., Sierro, F. J., Fuertes, M. A., Cros, L., and Trull, T. W.: Coccolithophore populations
697 and their contribution to carbonate export during an annual cycle in the Australian sector of the Antarctic zone,
698 *Biogeosciences*, 15, 1843-1862, BG, 2018.
- 699 Rigual Hernández, A. S., Trull, T. W., Nodder, S. D., Flores, J. A., Bostock, H., Abrantes, F., Eriksen, R. S., Sierro, F. J.,
700 Davies, D. M., Ballegeer, A. M., Fuertes, M. A., and Northcote, L. C.: Coccolithophore biodiversity controls carbonate
701 export in the Southern Ocean, *Biogeosciences*, 17, 245-263, doi: 10.5194/bg-17-245-2020, 2020a.
- 702 Rigual-Hernández, A. S., Trull, T. W., Flores, J. A., Nodder, S. D., Eriksen, R., Davies, D. M., Hallegraeff, G. M., Sierro, F.
703 J., Patil, S. M., Cortina, A., Ballegeer, A. M., Northcote, L. C., Abrantes, F., and Rufino, M. M.: Full annual monitoring
704 of Subantarctic *Emiliana huxleyi* populations reveals highly calcified morphotypes in high-CO₂ winter conditions,
705 *Scientific reports*, 10, 2594, doi: 10.1038/s41598-020-59375-8, 2020b.
- 706 Rivero-Calle, S., Gnanadesikan, A., Del Castillo, C. E., Balch, W. M., and Guikema, S. D.: Multidecadal increase in North
707 Atlantic coccolithophores and the potential role of rising CO₂, *Science*, 350, 1533-1537, doi: 10.1126/science.aaa8026,
708 2015.



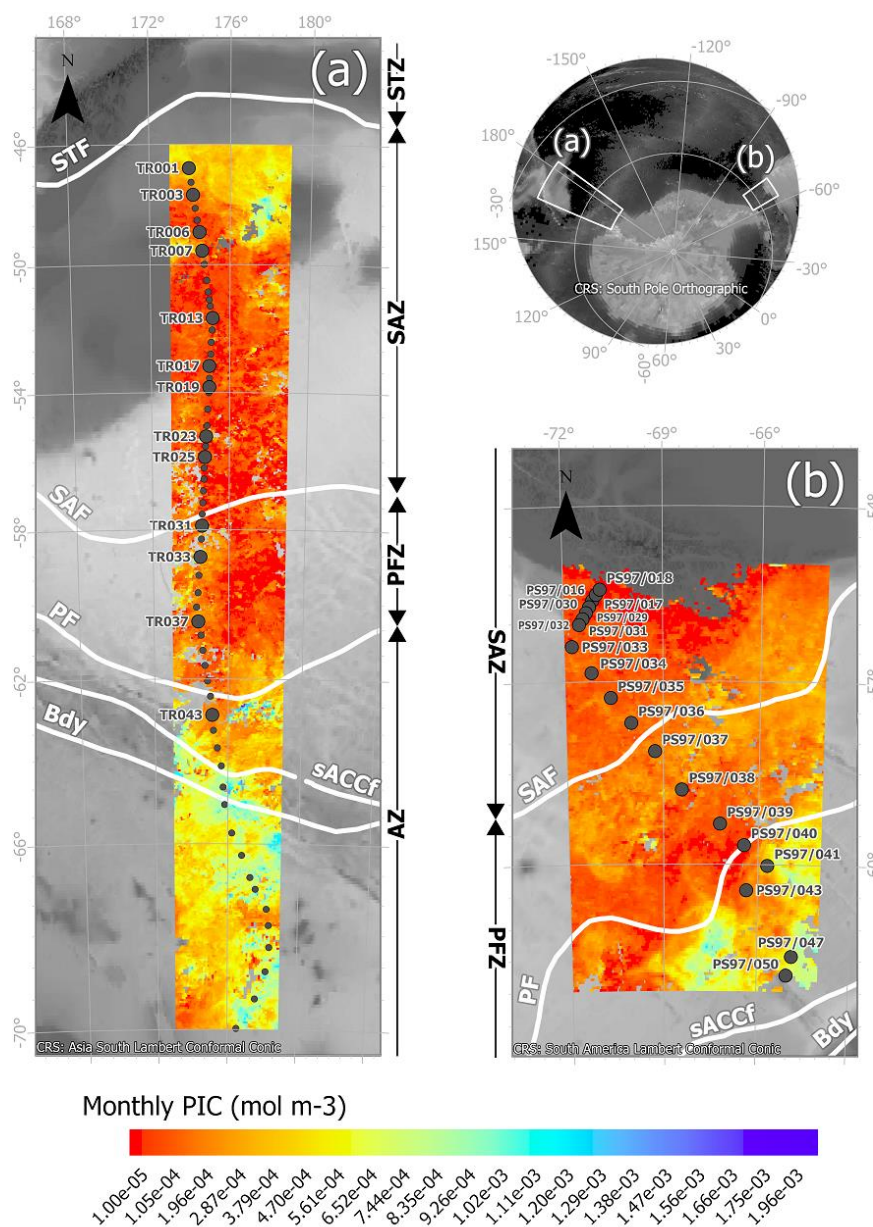
- 709 Rost, B., and Riebesell, U.: Coccolithophore calcification and the biological pump: response to environmental changes, in:
710 Coccolithophores: from molecular processes to global impact, edited by: Thierstein, H. R., and Young, J. R., Springer,
711 Berlin-Heidelberg, Germany, 99-125, 2004.
- 712 Saavedra-Pellitero, M., Baumann, K.-H., Flores, J.-A., and Gersonde, R.: Biogeographic distribution of living
713 coccolithophores in the Pacific sector of the Southern Ocean, *Marine Micropaleontology*, 109, 1-20, doi:
714 10.1016/j.marmicro.2014.03.003, 2014.
- 715 Saavedra-Pellitero, M., Baumann, K. H., Fuertes, M. Á., Schulz, H., Marcon, Y., Vollmar, N. M., Flores, J. A., and Lamy, F.:
716 Calcification and latitudinal distribution of extant coccolithophores across the Drake Passage during late austral summer
717 2016, *Biogeosciences*, 16, 3679-3702, doi: 10.5194/bg-16-3679-2019, 2019.
- 718 Salter, I., Schiebel, R., Ziveri, P., Movellan, A., Lampitt, R., and Wolff, G. A.: Carbonate counter pump stimulated by natural
719 iron fertilization in the Polar Frontal Zone, *Nature Geoscience*, 7, 885-889, doi: 10.1038/ngeo2285, 2014.
- 720 Samtleben, C. and Schröder, A.: Living coccolithophore communities in the Norwegian-Greenland Sea and their record in
721 sediments, *Marine Micropaleontology*, 19, 333-354, 1992.
- 722 Schindelin, J., Arganda-Carreras, I., Frise, E., Kaynig, V., Longair, M., Pietzsch, T., Preibisch, S., Rueden, C., Saalfeld, S.,
723 Schmid, B., Tinevez, J.-Y., White, D. J., Hartenstein, V., Eliceiri, K., Tomancak, P., and Cardona, A.: Fiji: an open-
724 source platform for biological-image analysis, *Nature Methods*, 9, 676-682, doi: 10.1038/nmeth.2019, 2012.
- 725 Schneider, C. A., Rasband, W. S., and Eliceiri, K. W.: NIH Image to ImageJ: 25 years of image analysis, *Nature Methods*, 9,
726 671-675, doi: 10.1038/nmeth.2089, 2012.
- 727 Shutler, J. D., Land, P. E., Brown, C. W., Findlay, H. S., Donlon, C. J., Medland, M., Snooke, R., and Blackford, J. C.:
728 Coccolithophore surface distributions in the North Atlantic and their modulation of the air-sea flux of CO₂ from 10 years
729 of satellite Earth observation data, *Biogeosciences*, 10, 2699-2709, doi: 10.5194/bg-10-2699-2013, 2013.
- 730 Siegel, H., Ohde, T., Gerth, M., Lavik, G., and Leipe, T.: Identification of coccolithophore blooms in the SE Atlantic Ocean
731 off Namibia by satellites and in-situ methods, *Continental Shelf Research*, 27, 258-274, doi: 10.1016/j.csr.2006.10.003,
732 2007.
- 733 Smyth, T. J., Moore, G. F., Groom, S. B., Land, P. E., and Tyrrell, T.: Optical modeling and measurements of a coccolithophore
734 bloom, *Appl. Opt.*, 41, 7679-7688, doi: 10.1364/AO.41.007679, 2002.
- 735 Smyth, T. J., Tyrrell, T., and Tarrant, B.: Time series of coccolithophore activity in the Barents Sea, from twenty years of
736 satellite imagery, *Geophysical Research Letters*, 31, doi: 10.1029/2004GL019735, 2004.
- 737 Suchéras-Marx, B., Viseur, S., Walker, C. E., Beaufort, L., Probert, I., and Bolton, C.: Coccolith size rules – What controls
738 the size of coccoliths during coccolithogenesis?, *Marine Micropaleontology*, 170, 102080, doi:
739 10.1016/j.marmicro.2021.102080, 2022.
- 740 Trull, T. W., Passmore, A., Davies, D. M., Smit, T., Berry, K., and Tilbrook, B.: Distribution of planktonic biogenic carbonate
741 organisms in the Southern Ocean south of Australia: a baseline for ocean acidification impact assessment,
742 *Biogeosciences*, 15, 31-49, doi: 10.5194/bg-15-31-2018, 2018.



- 743 Tyrrell, T., and Taylor, A. H.: A modelling study of *Emiliana huxleyi* in the NE atlantic, *Journal of Marine Systems*, 9, 83-
744 112, doi:10.1016/0924-7963(96)00019-X, 1996.
- 745 von Dassow, P., Díaz-Rosas, F., Bendif, E. M., Gaitán-Espitia, J. D., Mella-Flores, D., Rokitta, S., John, U., and Torres, R.:
746 Over-calcified forms of the coccolithophore *Emiliana huxleyi* in high-CO₂ waters are not preadapted to ocean
747 acidification, *Biogeosciences*, 15, 1515-1534, doi: 10.5194/bg-15-1515-2018, 2018.
- 748 Whitworth, T. I.: Zonation and geostrophic flow of the Antarctic circumpolar current at Drake Passage, *Deep Sea Research*
749 Part A. Oceanographic Research Papers, 27, 497-507, doi: 10.1016/0198-0149(80)90036-9, 1980.
- 750 Winter, A., Elbrächter, M., and Krause, G.: Subtropical coccolithophores in the Weddell Sea, *Deep Sea Research Part I:*
751 *Oceanographic Research Papers*, 46, 439-449, doi: 10.1016/S0967-0637(98)00076-4, 1999.
- 752 Winter, A., Henderiks, J., Beaufort, L., Rickaby, R. E. M., and Brown, C. W.: Poleward expansion of the coccolithophore
753 *Emiliana huxleyi*, *Journal of Plankton Research*, 36, 316-325, 10.1093/plankt/fbt110, 2014.
- 754 Yang, T. N., and Wei, K. Y.: How many coccoliths are there in a coccosphere of the extant coccolithophorids? A compilation,
755 *Journal of Nannoplankton Research*, 25, 7-15, 2003.
- 756 Young, J.: Coccobiom2 Macros, available from: <http://ina.tmsoc.org/nannos/coccobiom/Usernotes.html>, 2015 [Access 23
757 August 2017]
- 758 Young, J. R., and Ziveri, P.: Calculation of coccolith volume and its use in calibration of carbonate flux estimates, *Deep Sea*
759 *Research Part II: Topical Studies in Oceanography*, 47, 1679-1700, doi: 10.1016/S0967-0645(00)00003-5, 2000.
- 760 Young, J. R., Poulton, A. J., and Tyrrell, T.: Morphology of *Emiliana huxleyi* coccoliths on the northwestern European shelf
761 – is there an influence of carbonate chemistry?, *Biogeosciences*, 11, 4771-4782, doi: 10.5194/bg-11-4771-2014, 2014.
- 762



763

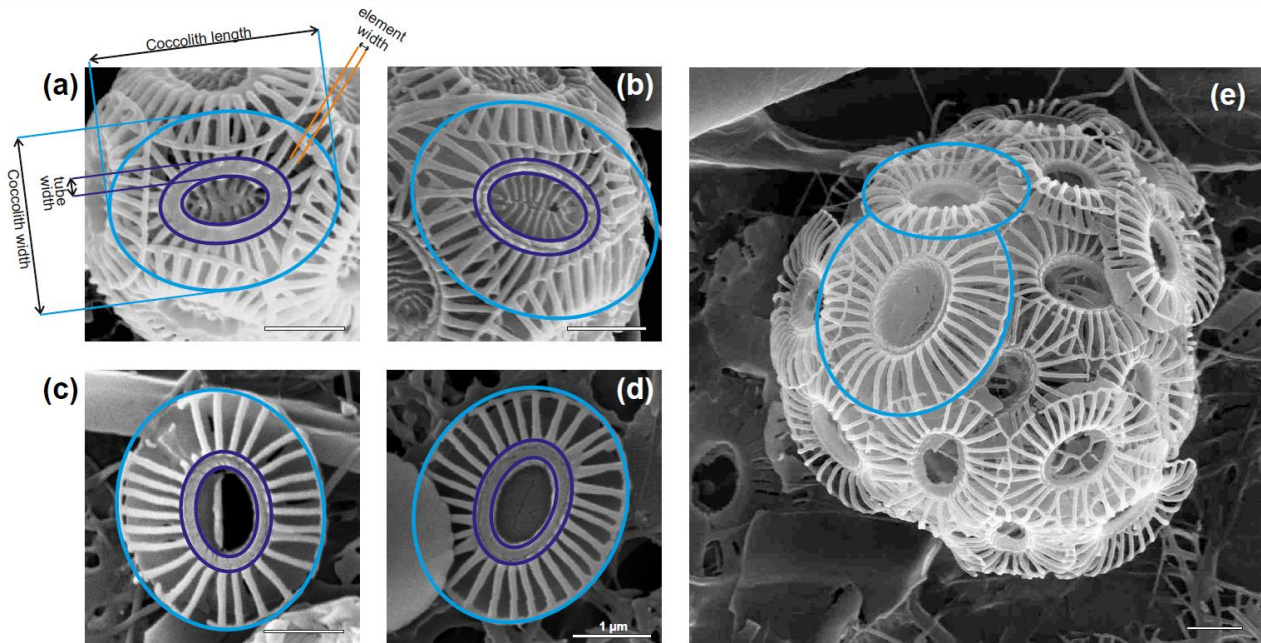


764
 765
 766
 767
 768
 769
 770
 771
 772
 773

Figure 1: Study area showing the location of the water samples retrieved from (a) the New Zealand transect, collected during the XX Italian Expedition from New Zealand to Antarctica on board R/V *Italica* (December 2004-January 2005) and (b) the Drake Passage transect, collected during Polarstern Expedition PS97 across the Drake Passage (February-March 2016). The maps show satellite-derived PIC values (NASA Ocean Biology Processing Group 2022) corresponding to (a) monthly mean over January 2005 and (b) monthly mean over February and March 2016, overlain on a bathymetry background (GEBCO Compilation Group, 2022). White lines indicate the ACC fronts (Orsi and Harris, 2019), from north to south these are: SAF (Subantarctic Front), PF (Polar Front), sACCf (Southern ACC Front) and Bdy (Southern Boundary). The Southern Ocean zones are labeled on the side of each map: STZ, Subtropical Zone; SAZ, Subantarctic Zone; PFZ, Polar Frontal Zone; AZ, Antarctic Zone.



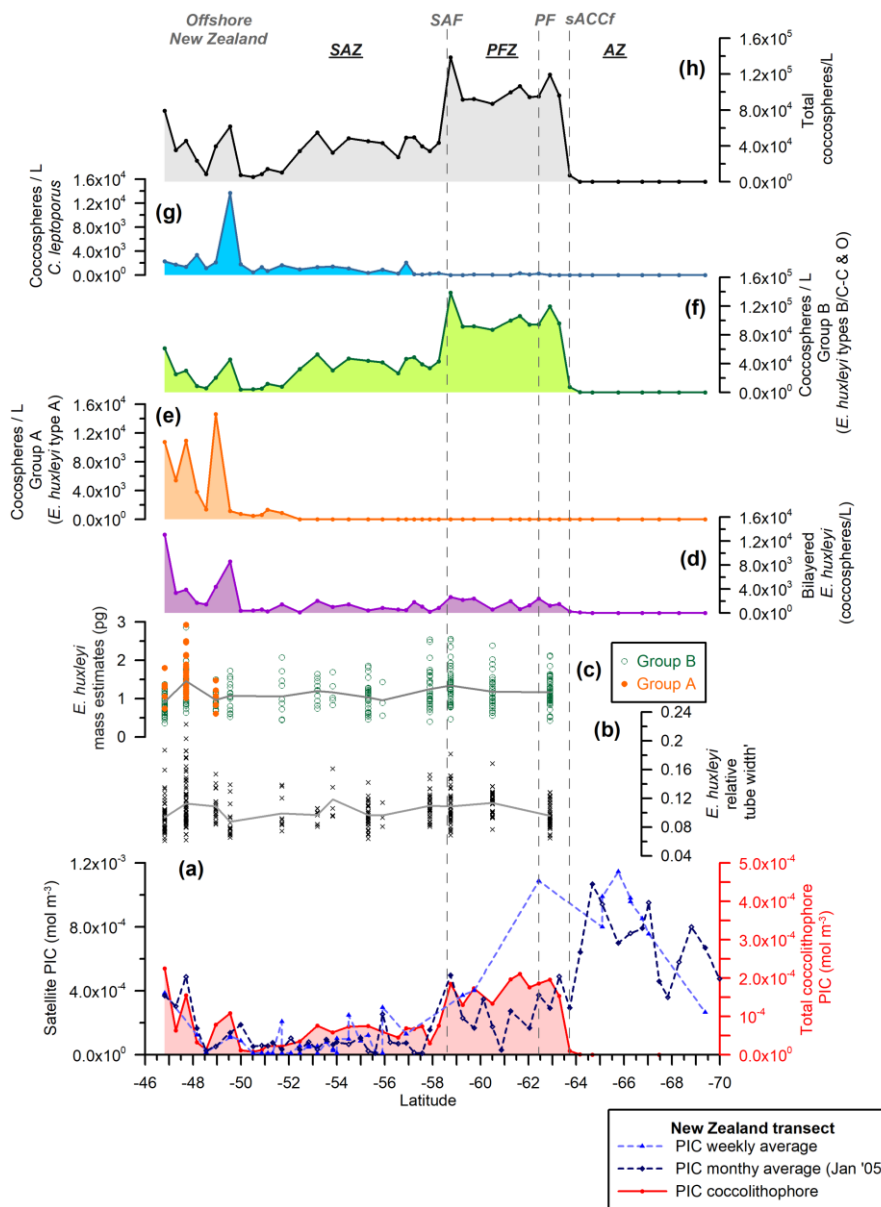
774



775
776
777
778

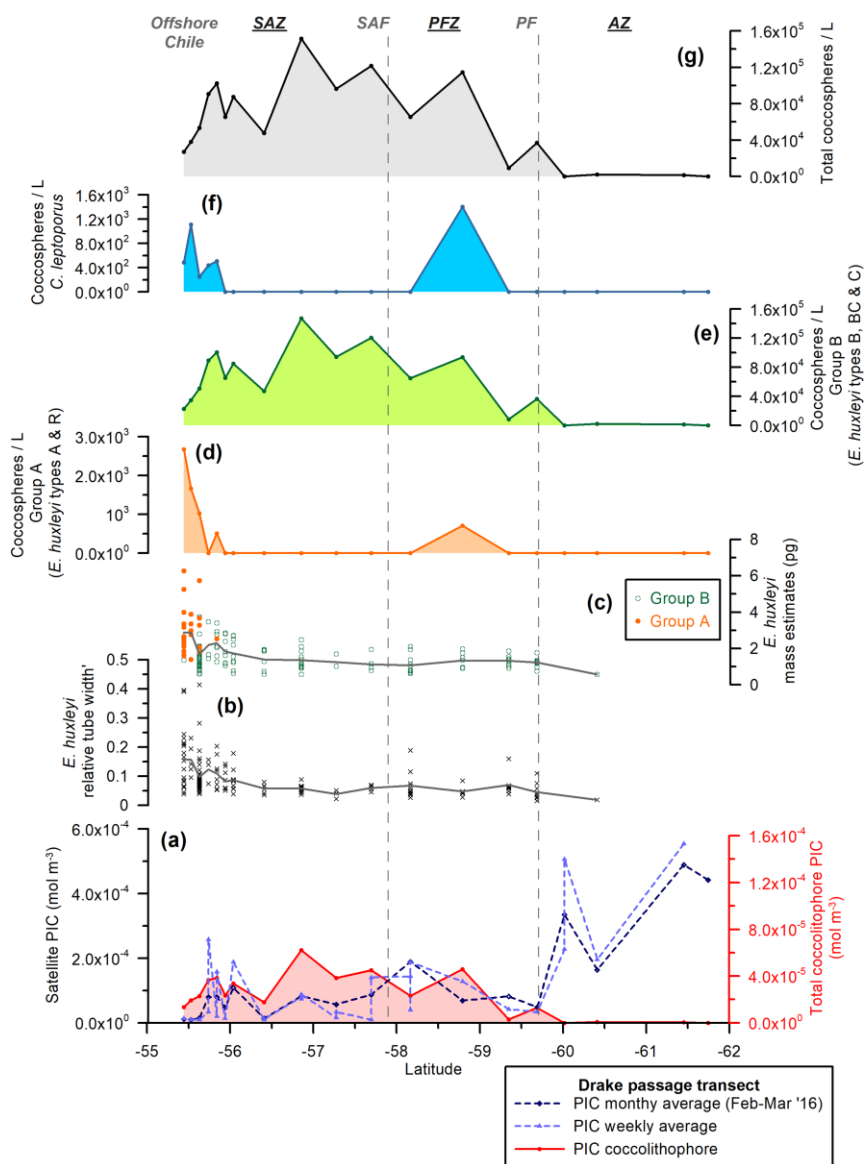
Figure 2: Parameters measured in *E. huxleyi* coccoliths (a, b) type A and (c, d, e) type O in plankton samples from the New Zealand transect. Note the coccolith size variation in (e) within the same coccosphere.

779



780
 781
 782
 783
 784
 785
 786
 787
 788
 789
 790

Figure 3: New Zealand transect showing (a) satellite-derived PIC values (NASA Ocean Biology Processing Group, 2022) corresponding to a monthly average (January 2005, dark blue dashed line with diamonds), weekly average (electric blue dashed line with triangles) and estimated total coccolithophore PIC (red line with dots), all in mol m⁻³, (b) *E. huxleyi* relative tube width² (average in gray), (c) *E. huxleyi* coccolith mass estimates (pg) (average in gray), (d) number of bilayered *E. huxleyi* (coccospheres/L), (e) number of *E. huxleyi* morphogroup A (coccospheres/L), (f) number of *E. huxleyi* morphogroup B (coccospheres/L), (g) number of *Calcidiscus leptoporus* (coccospheres/L), (h) Number of total coccolithophores (coccospheres/L) (Malinverno et al., 2015). Vertical dashed lines indicate some of the ACC fronts (Orsi and Harris, 2019): SAF (Subantarctic Front), PF (Polar Front) and sACCf (Southern ACC Front). The Southern Ocean zones are labeled as SAZ (Subantarctic Zone), PFZ (Polar Frontal Zone) and AZ (Antarctic Zone).

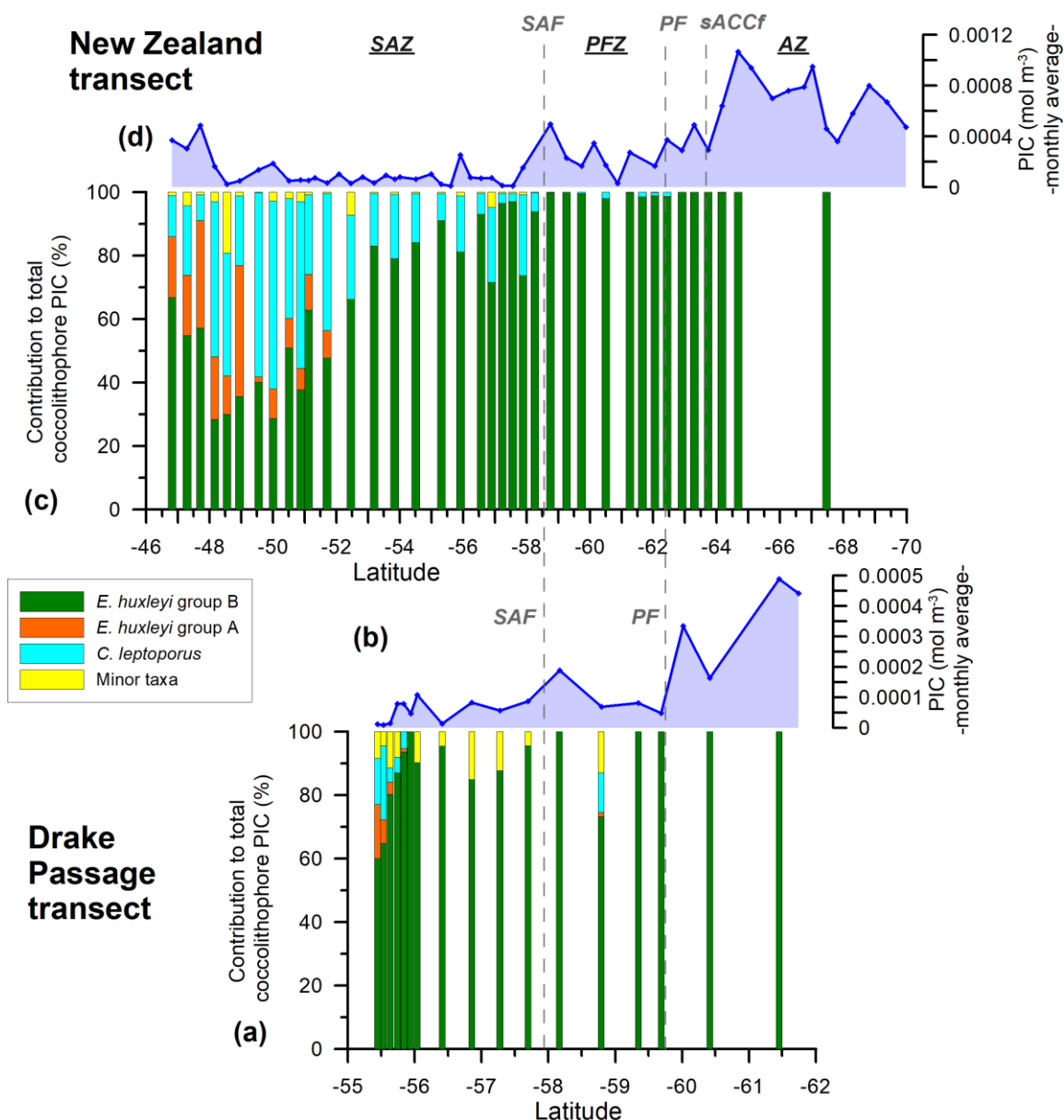


791
 792
 793
 794
 795
 796
 797
 798
 799
 800
 801

Figure 4: Drake Passage transect showing (a) satellite-derived PIC values (NASA Ocean Biology Processing Group, 2022) corresponding to a monthly average (February and March 2016, dark blue dashed line with diamonds), weekly average (electric blue dashed line with triangles) and estimated total coccolithophore PIC (red line with dots), all in mol m^{-3} , (b) *E. huxleyi* relative tube width' (average in gray), (c) *E. huxleyi* coccolith mass estimates (pg) (average in gray), (d) number of *E. huxleyi* morphogroup A (coccospheres/L), (e) number of *E. huxleyi* morphogroup B (coccospheres/L), (f) number of *Calcidiscus leptoporus* (coccospheres/L), (g) Number of total coccolithophores (coccospheres/L) (Saavedra-Pellitero et al., 2019). Vertical dashed lines indicate some of the ACC fronts (Orsi and Harris, 2019): SAF (Subantarctic Front) and PF (Polar Front). The Southern Ocean zones are labeled as SAZ (Subantarctic Zone), PFZ (Polar Frontal Zone) and AZ (Antarctic Zone).



802

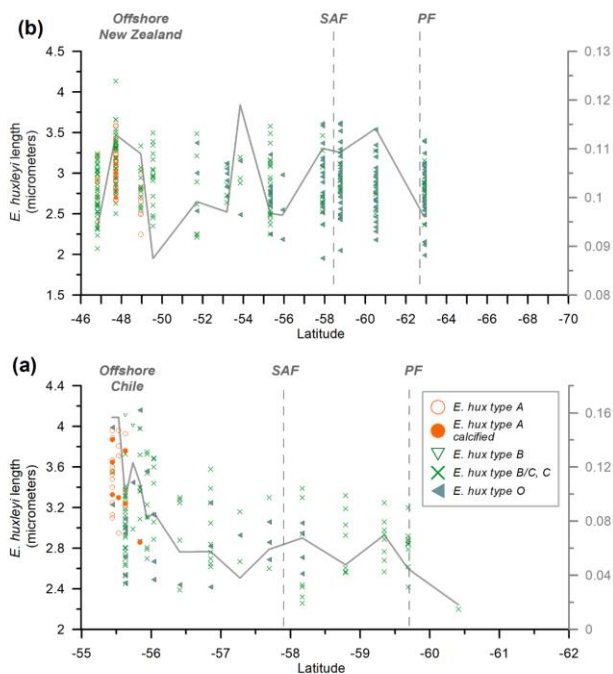
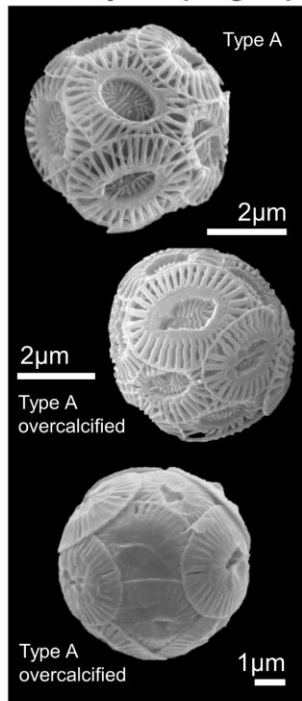


803
 804
 805
 806
 807
 808
 809
 810
 811
 812
 813

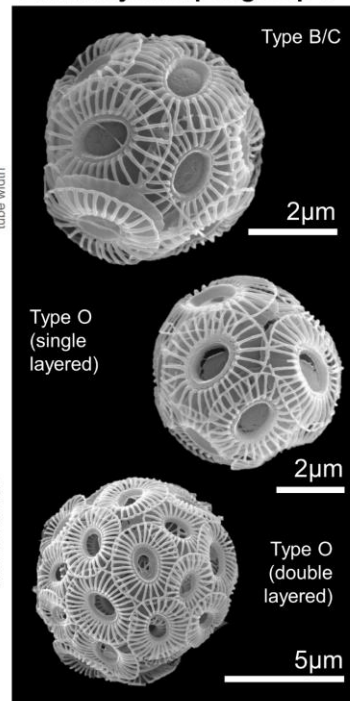
Figure 5: New Zealand and Drake Passage transects showing (a, c) the relative PIC contribution of the different nannofloral taxa (*E. huxleyi* morphogroups A and B, *Calcidiscus leptoporus* and minor species) to the estimated coccolithophore PIC; (b, d) satellite-derived PIC values (NASA Ocean Biology Processing Group 2022) corresponding to a monthly average (February and March 2016, dark blue line with diamonds) in mol m⁻³. Vertical dashed lines indicate some of the ACC fronts (Orsi and Harris, 2019): SAF (Subantarctic Front) and PF (Polar Front). The Southern Ocean zones are labeled as SAZ (Subantarctic Zone), PFZ (Polar Frontal Zone) and AZ (Antarctic Zone).



***E. huxleyi* morphogroup A**



***E. huxleyi* morphogroup B**

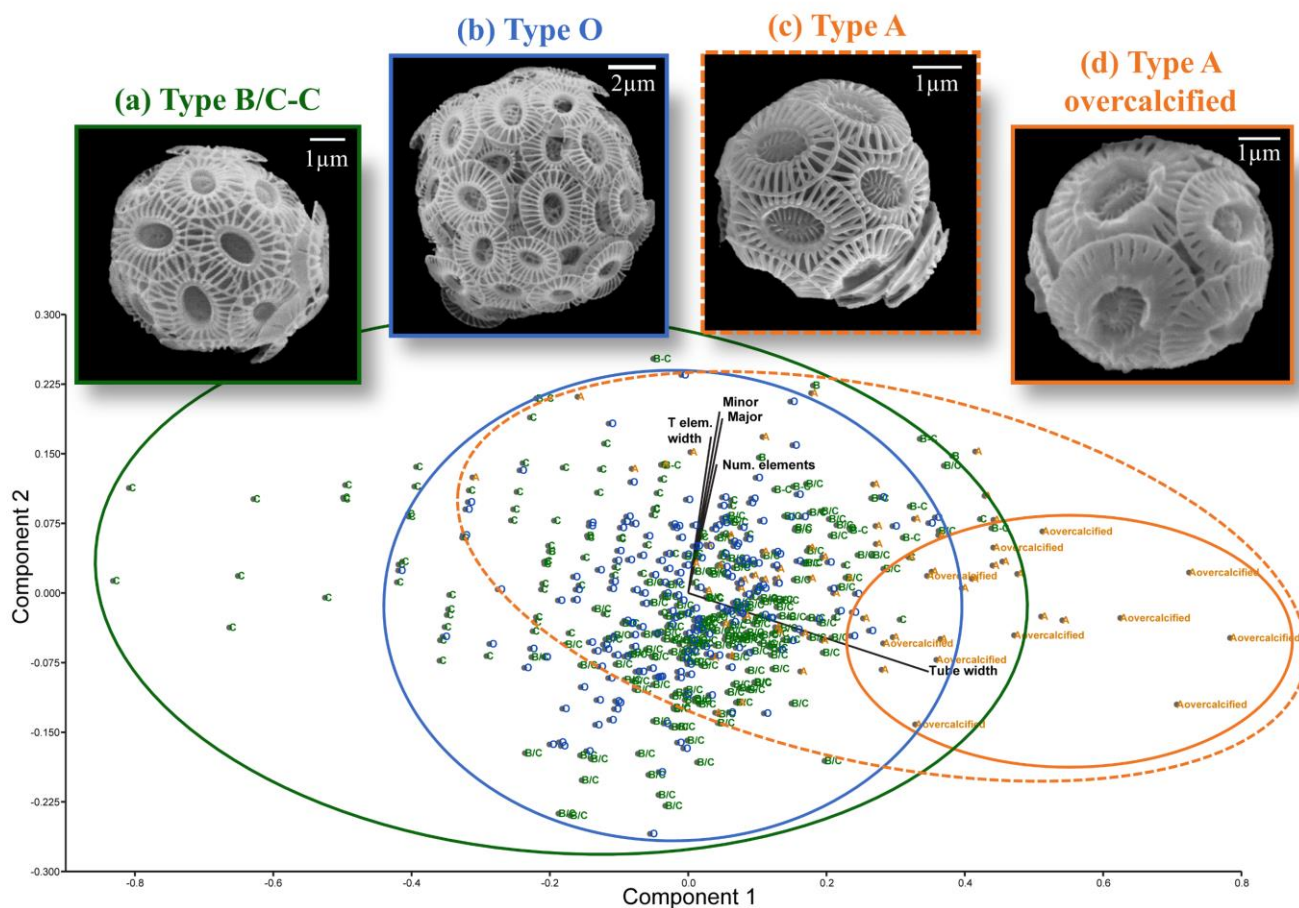


814
 815
 816
 817
 818
 819
 820
 821

Figure 6: *Emiliana huxleyi* length (in µm) (indicated with different symbols depending on the type, and different colors depending on the morphogroup) and averaged relative tube width' (gray line) in (a) the Drake Passage and (b) New Zealand transects. On the left-hand side: pictures of coccospheres of *E. huxleyi* type A (within the morphogroup A) showing different degrees of calcification and on the right-hand side pictures of type B/C as well as type O belonging to the morphogroup B. All the coccospheres are from the New Zealand transect, except for the left bottom one, which was retrieved offshore of Chile.



822
823
824

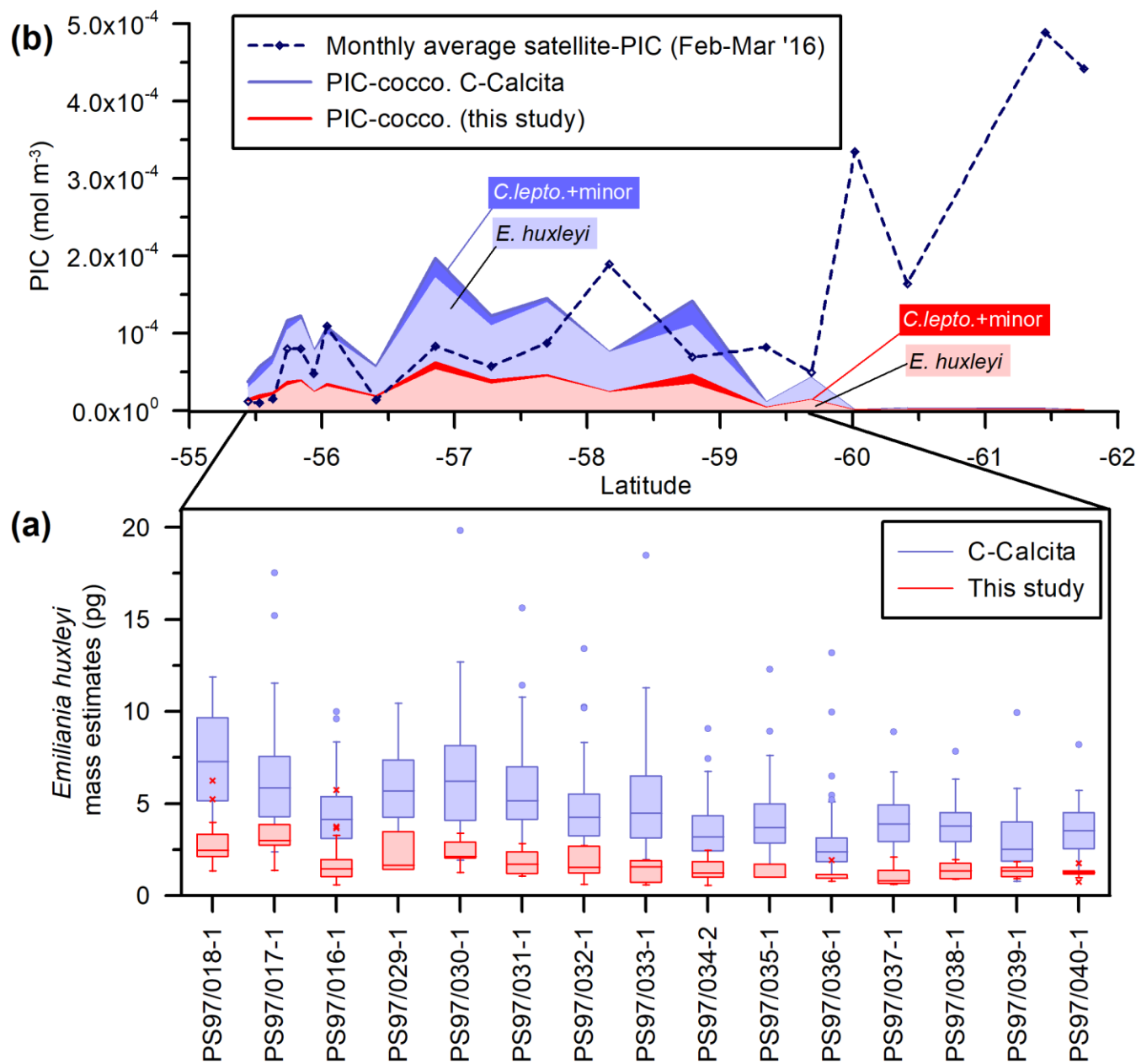


825
826
827
828
829
830
831
832

Figure 7: Principal component analysis (PCA) of the *E. huxleyi* morphometric dataset (including samples from both transects), log-transformed. This includes the coccolith length (major), the coccolith width (minor), the distal shield element width, the number of T-elements and the tube width measurements. Each coccolith measured has been labeled with its morphotype: A, A overcalcified (both in orange), B, B/C-C (both in green) and O (in blue). All the SEM pictures of coccospheres are from samples retrieved in the Drake Passage transect except for (c), which is from the New Zealand transect.



833
834

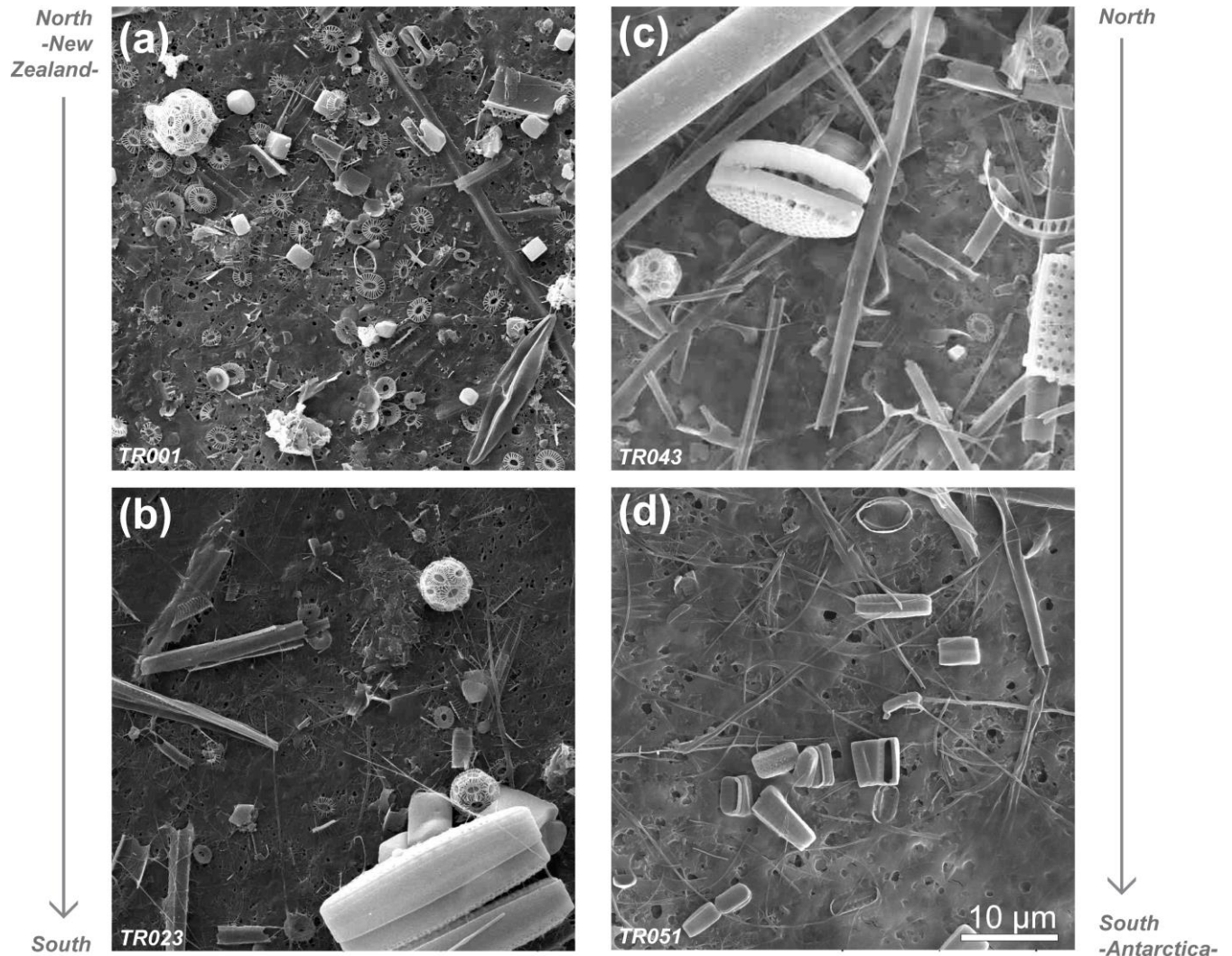


835
836
837
838
839
840
841

Figure 8: Drake Passage latitudinal transect showing (a) coccolith mass estimates box plots (in pg): in red for this study (outliers are indicated with “x”) and blue for Saavedra-Pellitero et al. (2019) (outliers are indicated with a dot); (b) monthly average satellite-derived PIC values (dark blue dashed line with diamonds) and estimated coccolithophore PIC (all in mol m⁻³). Contributions of different coccolith taxa have been indicated (*C.lepto.* = *Calcidiscus leptoporus*).



842



843
844
845
846
847
848

Figure 9: SEM pictures of samples retrieved in the Subantartic Zone (a, b) and south of the Polar Front (c, d) in the New Zealand transect.



849
850
851
852
853

Table 1: Length, Ks and number of coccoliths per coccosphere used in this work for the New Zealand transect and the Drake Passage transect. (*) Indicates an average of the number of coccoliths per coccosphere.

Coccolithophore species	Length (µm) New Zealand	Length (µm) Drake passage	Source	Ks	Source	Number of coccoliths per coccosphere N. Zealand	Number of coccoliths per coccosphere Drake P.	Source
<i>Calcidiscus leptoporus</i> spp. <i>leptoporus</i>	5	5	This work (biometries offshore N. Zealand)	0.08	Young and Ziveri (2000)	15	15	Kleijne (1993)
<i>Emiliana huxleyi</i> group A (average value)	2.95	3.49	This work	0.03	This work	15 single layered, 35 double layered	25 (*)	This work (own observations)
<i>Emiliana huxleyi</i> A overcalcified				0.04	Young and Ziveri (2000)			
<i>Emiliana huxleyi</i> A (normal)				0.02	Young and Ziveri (2000)			
<i>Emiliana huxleyi</i> group B (average value)	2.87	2.98	This work	0.02	Young and Ziveri (2000)			
<i>Emiliana huxleyi</i> B-B/C-C				0.02	Young and Ziveri (2000)			
<i>Emiliana huxleyi</i> O				0.015	This work			
<i>Gephyrocapsa muelleriae</i>	3.9	3.9	Young and Ziveri (2000)	0.05	Young and Ziveri (2000)	15	15	Samtleben & Schroder (1992)
<i>Syracosphaera</i> spp.	2.2	5.5	Young and Ziveri (2000)	0.03	Young and Ziveri (2000)	25	25	Okada & McIntyre (1977)
Minor taxa			Young and Ziveri (2000)		Young and Ziveri (2000)			Yang & Wei (2003)

854
855
856



857
 858
 859
 860
 861

Table 2. Summary of PIC time resolution and span. ()** The first 8-day period of each year always begins with January 1, the second with January 9, the third with January 17, etc. The final "8-day" composite of each year comprises only five days in non-leap years (27 - 31 December) or six days in leap years (26 - 31 December) (NASA Ocean Biology Processing Group, 2018).

Transect	Drake passage transect		New Zealand transect	
<i>File time period</i>	<u>Time span</u>	<u>Num. of files</u>	<u>Time span</u>	<u>Num. of files</u>
<i>Daily timestamp</i>	15-02-2016 / 05-03-2016	20	22-12-2004 / 06-01-2005	16
<i>8-daily timestamp (**)</i>	10-02-2016 / 12-03-2016	4	26-12-2004 / 08-01-2005	2
<i>Monthly timestamp</i>	01-12-2004 / 31-01-2005	2	01-02-2016 / 31-03-2016	2

862